Heat mitigation in basal compacted clay liners in municipal solid waste landfills

Abstract

In municipal solid waste (MSW) landfills, biodegradation of the organic MSW fraction results in elevated waste and basal liner temperatures which have the potential to cause the clay component of the basal liner to experience severe moisture loss over time and eventually undergo desiccation cracking. Cracking of the basal liner's clay component would result in an uncontrolled release of contaminants into the surrounding environment and ultimately give rise to a variety of major environmental concerns. Accordingly, this study examined the variation of temperature-moisture profiles along the depth of a compacted clay liner (CCL) exposed to different constant elevated waste temperatures (CETs) in the absence and presence of two heat reduction techniques, respectively. Rockwool insulation layers with varying thicknesses and galvanized steel cooling pipes with varying flowrates were introduced separately as the two heat reduction techniques. Introduction of both techniques led to a significant attenuation of the temperature rise and desiccation experienced by the CCL in the face of different CETs. An increase in rockwool thickness increments led to a progressive reduction of CCL temperature, while an increase in flow rate under turbulent condition did not have a significant influence on the temperature and desiccation reduction of the CCL. Nevertheless, the present study certainly highlights the potential of the two proposed heat reduction techniques to minimize desiccation and consequently increase the service life of CCLs exposed to different elevated temperatures in MSW landfills.

Keywords: Waste**;** compacted clay liner**;** temperature; desiccation; rockwool; cooling pipe

1. Introduction

The waste stored within a municipal solid waste landfill (MSWL) is typically isolated from the surrounding environment using a liner built into the base of the landfill, which essentially functions as a barrier between the environment and the municipal solid waste (MSW). The prime purpose of a basal liner is to prevent the migration of leachate present within the MSW into groundwater and protect it from contamination. Over time, the exothermic reactions related to aluminum production waste, incinerator ash, landfilled hot wastes, iron waste, bottom ash, tires, flue gas desulfurization gypsum, steel mill slag, petroleum coke, lime kiln dust, fluidized bed combustion residues, dried wastewater sludge and biodegradation of the organic content generates heat, which eventually leads to elevated waste and basal liner temperature [1, 2]. Researchers have reported waste temperatures of 35°C-135°C and basal liner temperatures of 30°C-70°C in the past [2-9]. Meanwhile, the groundwater table is known to possess a relatively cool temperature of 5 – 25°C [10-12]. Consequently, the significant temperature difference between the heated basal liner and the cool groundwater table leads to the inevitable development of thermal gradients across the liner and the subsoil as heat flows downward from the liner (high-temperature region) to the groundwater table (low temperature region) as per the second law of thermodynamics.

Thermal gradients in turn trigger the downward diffusion of water vapour from the warmed basal liner towards the cooler groundwater table (where it condenses), owing to the vapour density dependence on temperature. The migration of water vapour results in a significant reduction of moisture content in the warmed liner and leads to the development of capillary pressure gradients across the liner. The capillary pressure gradient then causes the liquid water to flow upwards in an attempt to balance the downward flux of water vapour. The reduced water content owing to downward vapour diffusion results in reduced unsaturated hydraulic conductivity which ultimately limits the volume of liquid water that reaches the warm

liner. Ultimately, the inability of the upward water flux to balance the downward vapour diffusion flux causes the clay component of the liner to experience desiccation cracking. This process is accelerated if the basal liner comprises a geomembrane, since the geomembrane (due to its impermeability) limits the transport of water vapour to the liner's clay component from the top portion of the landfill [13-15]. Cracking of the basal liner's clay component would result in an uncontrolled release of leachate to the surrounding environment, which would ultimately give rise to a variety of major environmental concerns such as groundwater pollution, soil contamination, vegetation damage, and unpleasant odours etc. [16-19]. **Fig. 1** illustrates the basic desiccation mechanism of a liner exposed to elevated waste temperatures in a typical MSW landfill (note that the diagram does not include all landfill components for the sake of clarity and simplicity).

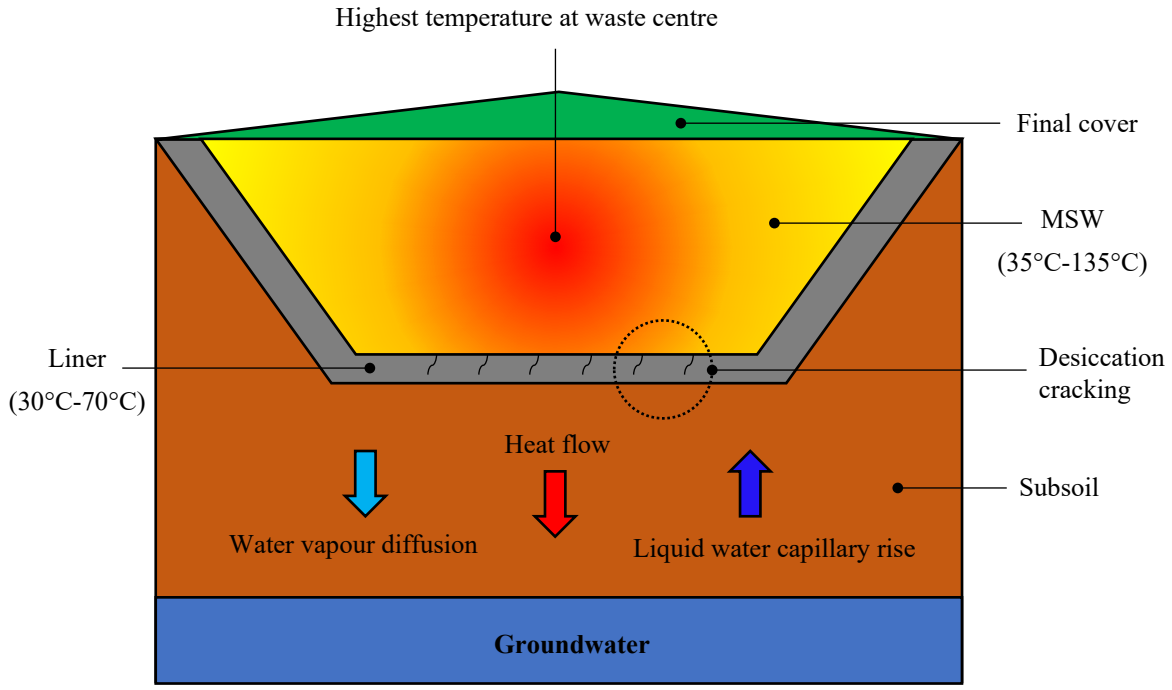

Fig. 1. Desiccation mechanism of liner exposed to elevated waste temperature

Deployment of landfill liners comprising geosynthetic components (such as geomembranes, geonets, geotextiles etc.) in "low- and middle-income" countries is often found to be economically unfeasible due to the high material and installation costs involved.

Moreover, the installation of liners comprising geosynthetic materials requires a very high level of quality control with regard to site preparation, installation, and protection control. Hence, the use of geosynthetic lining materials is generally not recommended in low- and middle-income countries [20-23]. As a result, in such countries, compacted clay liners (CCLs) are found to be the most commonly used landfill liner system. While CCL is less expensive, it also possesses the required qualities of a suitable liner, such as good attenuation capacity and low permeability. Moreover, the deployment of CCLs as landfill liners in low- and middle-income countries usually enables the utilization of locally available materials, workmanship, equipment, and technology [20, 23, 24].

A total of 125 countries out of 179 surveyed countries in the world (i.e., nearly 70%) fall under the low- and middle-income categories, when classified by the development level of gross national income per capita (GNI) [25]. Hence, it is safe to presume that at present, a large portion of the world most likely still employs CCLs as their default landfill liner. Yet, surprisingly, studies that have examined the effect of elevated waste temperatures on CCL temperature-moisture distributions in landfills were found to be incredibly scarce within the literature. Holzlöhner [26] applied a temperature gradient to a heavy clay column compacted within a polyvinyl chloride tube and observed that the clay column shrank as a result of desiccation to such an extent that it was separated from the top and sides of the tube. Holzlöhner et al. [27] subjected a range of soils (from sand-silt to high-plasticity clay) to temperature gradients to calculate diffusion coefficients under the effect of temperature and moisture gradients. Abdulrahman [28] exposed compacted clay samples to elevated temperatures for over two months and found that the hydraulic conductivity rises with increasing temperature. Abdulrahman [28] attributed the observed permeability rise to micro-crack generation (caused due to desiccation) and increased viscosity of the permeant that aided its movement through the clay matrix. However, none of the studies conducted by Abdulrahman [28]; Holzlöhner

91 [26]; and Holzlöhner et al. [27] involved a comprehensive investigation into the variation of
92 temperature-moisture profiles along the depth of the clay liner when exposed to different
93 elevated waste temperatures within a MSW landfill.

94 Over the past few years, researchers have also proposed several methods to reduce
95 heating and desiccation of basal lining systems when exposed to elevated temperatures in
96 various waste containment facilities. El-Zein et al. [29] and Yu et al. [30] showed that
97 increasing the bentonite mass per unit area of a GCL (by approximately 10%) leads to a
98 reduction in its desiccation crack area. Bouazza et al. [31]; El-Zein et al. [29]; and Yu, El-Zein
99 [32] discovered that the existence of an air-filled gap between the heat source and the liner
100 leads to an attenuated heat flow across the liner system. El-Zein et al. [29]; and Yu, El-Zein
101 [32] specifically observed that the presence of an air-filled gap leads to a reduction in
102 desiccation crack width in a GCL exposed to elevated temperatures. Yu et al. [33] found that
103 while polymer-enhancement reduces the desiccation cracking of a GCL exposed to moderate
104 temperatures, it is ineffective at higher temperatures. Yu, El-Zein [34] achieved GCL hydration
105 via artificial irrigation and hydraulic separation of the liner system from the underlying subsoil,
106 which consequently led to complete prevention of its desiccation when exposed to elevated
107 temperatures. Hoor [35]; Hoor et al. [4]; Rowe et al. [36]; and Rowe et al. [37] numerically
108 examined the installation of a horizontal cooling pipe array beneath the waste at the base of the
109 landfill and found that it leads to a reduction in liner surface temperature. Moreover, numerical
110 studies conducted by Hoor [35]; Hoor, Rowe [38]; Hoor, Rowe [39]; and Rowe, Hoor [40]
111 showed that the theoretical introduction of a suitable insulation layer of either sand, geofoam,
112 shredded tires, tire chips or soil within a liner system could substantially reduce its temperature
113 when exposed to high waste temperatures.

114 However, the above works that examined the effect of cooling pipes and insulation
115 mechanisms on heat reduction in landfill basal liners were strictly numerical and require

116 experimental evidence to confirm their respective efficacies. Thus far, to the authors'
117 knowledge, no experimental work has been carried out to examine the heat reduction effect of
118 introducing an insulation layer or a cooling pipe system directly on top of a landfill basal lining
119 system when exposed to elevated waste temperatures. Therefore, the objective of this study
120 was to conduct a laboratory investigation into the variation of temperature-moisture profiles
121 along the depth of a CCL exposed to elevated waste temperatures and examine the potential
122 effectiveness of utilizing either cooling pipes or an insulation layer on the reduction of the
123 CCL's temperature and consequently, its desiccation. Accordingly, a series of laboratory
124 experiments were conducted, where a CCL block was exposed to elevated temperatures of
125 40°C-70°C. Variations of temperature-moisture profiles within the CCL in the absence and
126 presence of heat reduction techniques were then assessed.

127 **2. Materials**

128 **2.1. Compacted Clay Liner (CCL)**

129 Marine clay, which was employed as the CCL for the present study, is generally known
130 to occur in the form of deposits along many coastal regions around the world [41]. In Malaysia,
131 marine clay is abundantly available along the coastal regions of the Peninsular, particularly in
132 regions such as Johor, Malacca, Klang, Jeram, Penang, and Alor Star [42]. Several researchers
133 have recommended the use of marine clay as a liner material based on its physical properties,
134 low hydraulic conductivity, heavy metal adsorption capacity, natural desiccation cracking
135 resistance, heavy metal retention capability and the potential to function as a geosorbent that
136 retains pathogenic bacteria in landfill leachate [43-48]. At present, marine clay is utilized as a
137 landfill liner in Malaysia, Singapore and Japan [49-51].

138 For the present study, marine clay samples were obtained from the vicinity of the
139 coastal region located in Kampung Dungun, 45800 Jeram, Selangor, Malaysia (3°11'53.7"N,
140 101°18'23.4"E). The basic geotechnical and thermal properties of the collected marine clay are

provided in **Table 1**. It should be mentioned here that all water contents mentioned in **Table 1** were calculated using the gravimetric method, and that the thermal properties reported were calculated for marine clay compacted (using the mini-compaction apparatus) at a moisture content that was 2% wet of optimum, which was the moisture content that was used to prepare marine clay for all experiments in this research [52]. In accordance with the British Standard Classification System (BSCS), marine clay was classified as a clay of high plasticity (CH). An image of crushed marine clay is provided in **Fig. 2(a).**

Table 1. Basic geotechnical and thermal properties of marine clay

Soil Properties	**Value**
Natural Water Content (%)	60.46
Specific Gravity	2.48
Atterberg Limits	
Liquid limit (%)	66
Plastic limit (%)	31
Plasticity Index (%)	35
Organic Content (%)	3.79
Activity	0.81
British Standard Classification System (BSCS)	CH
Maximum Dry Density (MDD) (g/cm^3)	1.54
Optimum Moisture Content (OMC) (%)	24.20
Linear shrinkage (%)	14.2
Particle size distribution (%)	
Gravel	-
Sand	12
Silt	45
Clay	43
Fines Content (Clay + Silt)	88
Unconfined Compressive Strength (UCS) (kPa)	704
Thermal Properties	
Thermal conductivity (W/m°C)	1.160
Volumetric Heat capacity (MJ/m^3°C)	1.893
Thermal Diffusivity (mm^2/s^2)	0.613
Thermal Resistivity (°C.cm/W)	86.230

2.2. Cooling pipe

A few essential factors were carefully considered prior to selecting the material that was used to fabricate the cooling pipe network. Firstly, as mentioned previously, majority of the nations that utilize compacted clay as their landfill barrier system without the use of geosynthetic component(s) fall under the low- and middle-income category. Hence for such nations to successfully implement the cooling pipe technique as a viable solution for heat reduction in CCLs, it is vital that the pipe material be of low cost. Secondly, it is crucial that the chosen pipe material be readily available in the market for the construction stage of the cooling pipe system and also for emergency instances where certain pipes are found to be damaged beyond repair and thus require immediate replacement. Thirdly, it is essential that the chosen pipe material possessess a high thermal conductivity for an effective heat exchange between the coolant and the surrounding medium that the pipe network would be buried in. Finally, it is required that the pipe material be resistant to corrosion. Since galvanized steel (GS) meets all of the above-mentioned criteria, it was thus chosen to fabricate the cooling pipe network [53-57]. **Fig. 2(b)** shows the heat exchange component of the cooling pipe network fabricated using GS.

2.3. Thermal insulator

In this study, rockwool is proposed as a potential thermal insulation material that can be safely deployed in MSW landfills to minimize CCL desiccation in the face of elevated waste temperatures due to three major reasons. Firstly it is a sustainable nature-based insulation material made of renewable volcanic stone. Secondly, it possesses a thermal conductivity 3 – 26 times lower than those of other liner insulation materials previously proposed by Hoor [35]; Hoor, Rowe [38]; and Hoor, Rowe [39]. Finally, rockwool is moisture resistant yet vapour permeable, meaning that while it resists water absorption by default, its vapour permeability permits water vapour to pass through and hydrate the CCL from the top, thus minimizing its

desiccation under elevated waste temperatures. Basic properties of the purchased rockwool boards are tabulated in **Table 2**.

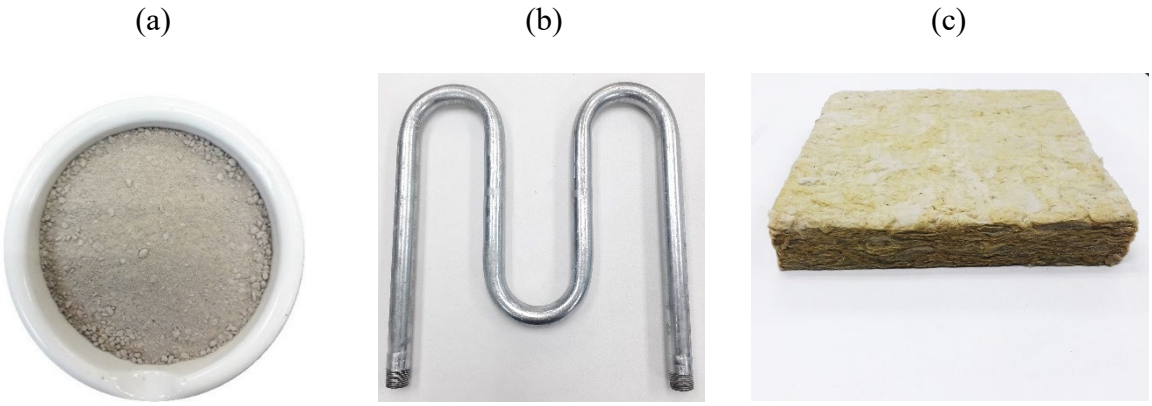

Fig. 2. Images of: (a) marine clay (crushed); (b) galvanized iron cooling pipe; (c) rockwool

Table 2 Basic properties of rockwool

Property	Value	Reference
Density (kg/m^3)	54.957	Measured (laboratory)
Thermal Conductivity (W/m.K)	0.028	Measured (KD2 Pro Analyzer)
Volumetric heat capacity (MJ/m^3.K)	0.127	Measured (KD2 Pro Analyzer)
Thermal diffusivity (mm^2/s)	0.218	Measured (KD2 Pro Analyzer)
Melting Point (°C)	> 1000°C	Manufacturer's specifications
R-value at 50mm thickness (m^2.K/W)	1.389	Manufacturer's specifications
Water Absorption (partial immersion) (kg/m^2)	1	Manufacturer's specifications
Water Vapor Absorption	< 0.04 Vol %	Manufacturer's specifications

3. Methodology

3.1. Cooling pipe design concept

The proposed cooling pipe system in the present study was inspired by heat exchanger designs suggested by Coccia et al. [58]; Hoor [35]; Hoor et al. [4]; Rowe et al. [36]; and Rowe et al. [37]. The concept entails the installation of an array of closed-loop horizontal pipes embedded within a thick sand protection layer (henceforth referred to as pipe sand layer or PSL) located directly above the CCL. A coolant being circulated through the pipe network at a designated flowrate will intersect the heat flow towards the CCL and absorb the heat from the sand. Fine sand particles with high thermal conductivity will ensure good contact with pipes

and facilitate the heat exchange process. Consequently, the magnitude of temperature experienced by the CCL will be significantly reduced. The heated coolant will then be transported to facilities outside the landfill where the heat energy will once again be extracted from the coolant and used for various applications, such as onsite use, preheating of domestic hot water, heating of greenhouses in winter, intensifying the evaporation of leachate collected in leachate ponds etc. [4, 35-37, 59]. Following heat extraction outside the landfill, the coolant will then be recirculated through the pipe system. Water is proposed as the coolant due to its low cost, low viscosity, availability and non-hazardous nature in the event of a leak.

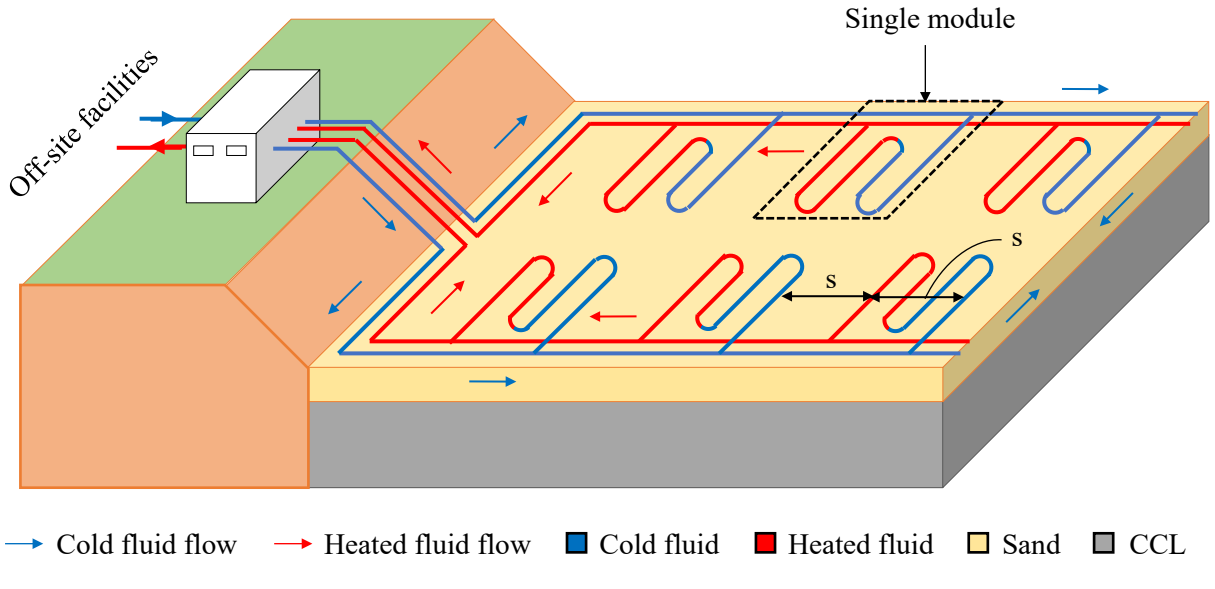

Fig. 3. Three-dimensional view of proposed cooling pipe configuration in a MSW landfill (s = intermodular/intramodular spacing)

Based on heat exchange principles, a pipe configuration that comprises alternating entry and return pipes is considered the most efficient arrangement [4]. Accordingly, a hypothetical three-dimensional illustration of the proposed pipe configuration (comprising a 4-pass module arrangement) installed within a MSW landfill is provided in **Fig. 3**. The design proposed in is purely *conceptual* in nature and the illustration in **Figs. 3** shows only a portion of the landfill in terms of length. Hence, a detailed design analysis would later be required to fully assess the practicality of installing the proposed pipe array system within a landfill. It was decided that

205 the pipe array (embedded within the sand layer) will be located below the leachate collection
206 system (LCS) due to two main reasons. Firstly, if placed below the LCS, the sand layer will
207 provide protection to the CCL from physical damages [36]. Secondly, if the sand layer with
208 the pipes were located above the LCS, significant volumes of leachate may enter the sand layer
209 and interfere with the heat exchange process. However, when located below the LCS, the
210 majority of the leachate will be collected by the leachate collection pipes and the leachate effect
211 on the heat exchange process will be minimized. A schematic cross-section diagram of a
212 landfill profile following installation of the cooling pipe system is provided in **Fig. 4(a)**.

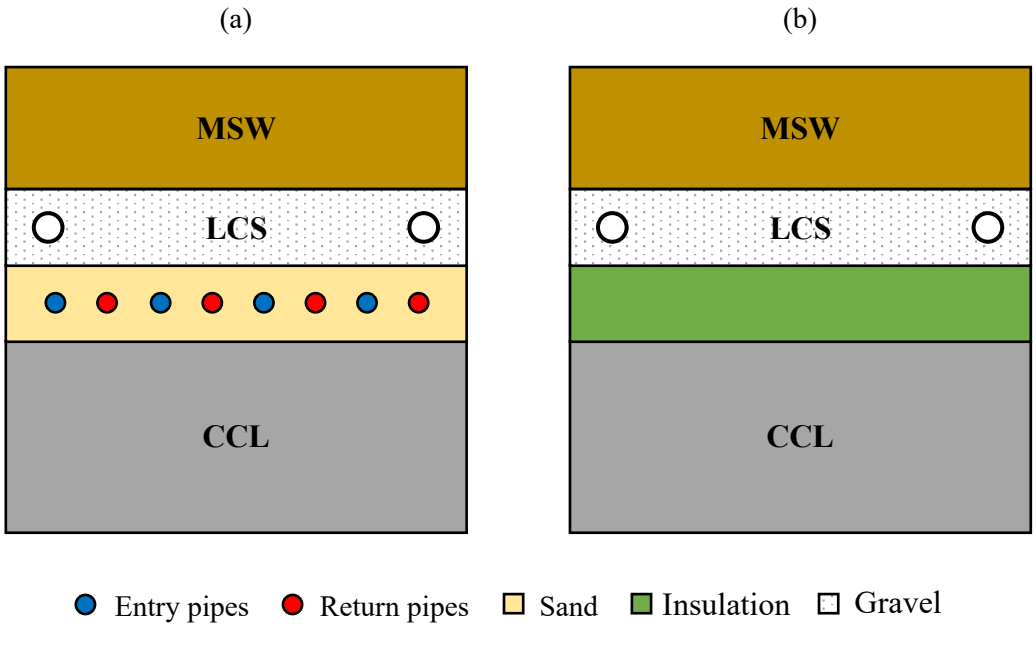

213

214 **Fig. 4.** Schematic landfill cross-section following installation of a: (a) cooling pipe system;
215 (b) insulation layer

216 **3.2. Insulation design concept**

217 The insulation design involves the installation of a rockwool layer directly above the
218 CCL and below the LCS. When located below the LCS, the rockwool layer will provide
219 protection to the CCL from physical damages [36]. Moreover, since the leachate collection
220 system is above the rockwool layer, the leachate will not accumulate on top of the rockwool
221 layer and disrupt its functionality. **Fig. 4(b)** presents the schematic diagram of a landfill cross-

section following installation of the rockwool insulation layer. The insulation design is merely *conceptual* in nature and will require the conduction of a detailed design analysis later, if deemed worthy of being implemented within a MSW landfill.

3.3. Sample preparation

Marine clay collected from the site possessed a natural (gravimetric) water content of 60.5% which rendered immediate crushing impossible. Hence, the clay was oven dried at 105°C for over 24 hours and then crushed using a mechanical grinder into fine particles. The crushed clay was passed through a 2.36 mm sieve and stored at room temperature in sealed polythene bags.

3.4. Experimental program

The experimental program examined the effect of implementing different heat reduction techniques on the temperature and desiccation reduction of a CCL block subjected to constant elevated waste temperatures. Accordingly, the experimental program was divided into three main subprograms, viz. *base case*, *cooling case* and *insulation case*. The *base case* involved subjecting the CCL to constant elevated waste temperatures in the absence of any heat reduction mechanisms, which simulated the present situation in MSW landfills. The *cooling* and *insulation cases* entailed the introduction of a cooling pipe network and a rockwool layer directly above a CCL subjected to constant elevated temperatures, respectively. For all cases, the required waste temperatures above the CCL were generated with the aid of an electric heat pad circuit. The conditions that were adopted for each experiment are tabulated in **Table 3** and the depicted via a flowchart in **Fig. 5**.

Table 3. Summary of experimental conditions

ID	Experiment	CET (°C)	Pipe material	Coolant flowrate (m^3/h)	Insulation material	Insulation thickness (mm)
1	Base case	40	-	-	-	-
2	Base case	55	-	-	-	-

3	Base case	70	-	-	-	-
4	Cooling case	40	GS	0.75	-	-
5	Cooling case	70	GS	0.75	-	-
6	Cooling case	70	GS	1.5	-	-
7	Insulation case	40	-	-	Rockwool	20
8	Insulation case	40	-	-	Rockwool	35
9	Insulation case	40	-	-	Rockwool	50
10	Insulation case	70	-	-	Rockwool	20
11	Insulation case	70	-	-	Rockwool	35
12	Insulation case	70	-	-	Rockwool	50

CET = Constant elevated temperature; GS = Galvanizeed steel

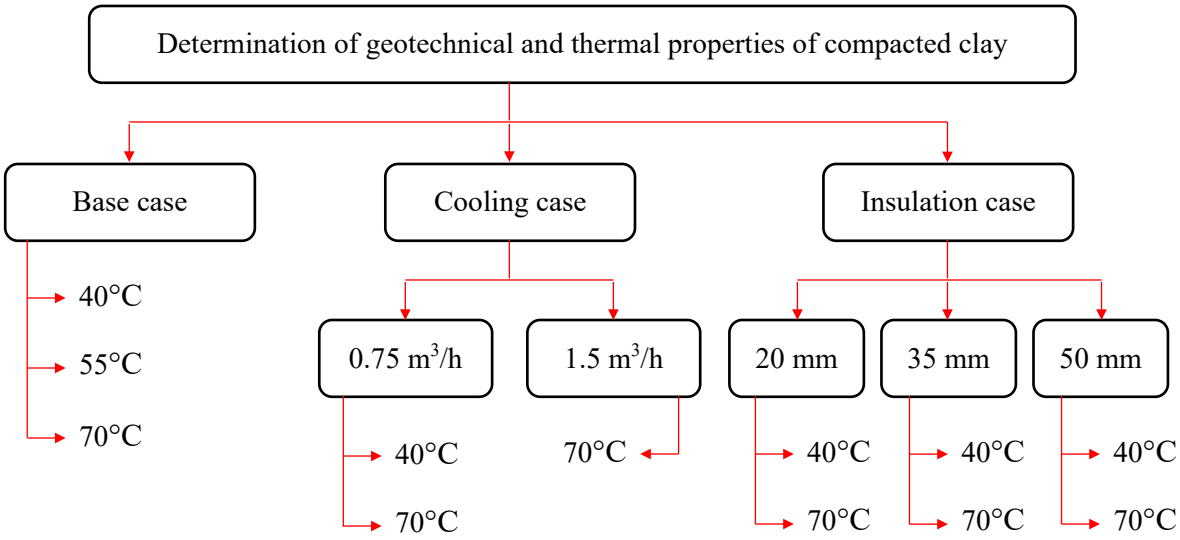

Fig. 5. Experimental flowchart

3.4.1. Heat generation mechanism

The circuit employed for the application of heat comprised a mica flat heater as the electric heat pad, a PT100 Resistance Temperature Detector (RTD) probe, a GT8 ATS 210 Proportional Integral Derivative (PID) controller and a 40 Amp Solid-State Relay (SSR). All circuit components were purchased from the company, Elmec Heaters and Controllers based in Chennai, India. As the first step of heat application, a fine dry sand layer, henceforth referred to as the temperature detection sand layer (TDSL), was placed over either the CCL, pipe sand layer (PSL) or rockwool insulation layer, depending on the experimental case. The heat pad was then placed on top of the TDSL and the RTD probe was inserted into the mid-region of

256 the TDSL. Subsequently, the heat pad and RTD probe were connected to the PID controller
257 and the SSR to form a closed circuit. Once the desired temperature was entered into the PID
258 controller, the TDSL temperature was continuously monitored by the PID controller via the
259 RTD sensor and maintained at the required temperature by switching the heat pad on and off
260 with the aid of the SSR. The top surface of the heat pad was insulated (referred to as *heat pad*
261 *insulation* or *HPI*) in order to minimize heat loss to the external environment. Since the TDSL
262 (a) was assigned a low thickness (25 mm), (b) was dry with minimal moisture variation and (c)
263 possessed a reasonably high thermal conductivity, it was presumed that the entire TDSL layer
264 was uniformly heated to the desired temperature during all experimental cases. Accordingly,
265 the TDSL served as the heated waste layer above the CCL.

266 **3.4.2. Base case**

267 Crushed and oven-dried clay was mixed with adequate water until a moisture content
268 that was 2% wet of its optimum moisture content (OMC) was attained, as typical of current
269 practice in the field [60, 61]. For compaction of the clay, it was decided that a compaction
270 energy equivalent to that of the reduced proctor test be delivered to the clay in order to be
271 conservative. The reduced proctor effort (356.7 kJ/m^3) corresponds to the minimum level of
272 compactive energy required for a typical soil liner [61, 62]. The lower the degree of soil
273 compaction, the higher the number of water-filled pores and the higher the water content
274 gradient. Consequently, the higher the potential for desiccation cracking [63]. During
275 compaction, a heavy metal plate was placed on the moist clay and the standard proctor rammer
276 was dropped onto the plate. The compaction energy delivered was approximately 383 kJ/m^3
277 which was slightly higher than that of the reduced proctor test in order to allow for energy
278 losses that occur when the hammer contacts the metal plate [52].

279 The clay was compacted in five lifts to a total height of 130 mm within a custom-
280 designed wooden tank that possessed a length and width of 300 mm each. The present study

thus employed a CCL volume which was 2.5 to 5 times the volume of soil columns subjected to elevated waste temperatures by researchers in the past [13, 28, 31, 33, 64, 65]. Despite the typical thickness of a CCL installed at the base of a landfill being equivalent to approximately 1 m, previous studies have repeatedly shown that when soil columns were subjected to high temperatures, it was the top region of the soil (particularly the upper 100 mm) that served as the critical zone for moisture and heat variation [31, 63, 69, 70]. Therefore, for the present study, only the top 110 mm of the CCL depth was examined for variation in temperature and moisture profiles along the depth. Accordingly, the CCL's top surface (i.e., the interface between TDSL and CCL) served as the reference datum for CCL depth and corresponded to a depth of 0 mm. Moreover, in accordance with the general sign convention, all depths below the CCL top surface were considered negative. Meanwhile, the 20 mm of excess clay below the first 110 mm of the CCL depth was simply included to simulate downward continuity of the CCL (similar to field conditions) and to prevent the base of the wooden tank from interfering with the temperature and moisture readings measured at a depth of 110 mm from the CCL's top surface.

Following compaction of each layer, samples from the CCL's mid-region were acquired for the determination of initial water content. The wooden tank was assigned a significant wall thickness of 2 cm in order to ensure that it provided the CCL with good insulation that minimized heat transfer between the internal contents of the tank and the external environment. Moreover, the tank was coated with automotive paint to minimize the absorption of soil moisture by wood. Type T and J thermocouple probes of 1.5 mm diameter were inserted into the CCL at designated depths through pre-drilled holes in the tank, with the three uppermost thermocouples being more closely spaced to capture the steep variation of temperature close to the top surface. The thermoocouples were purchased from OMEGA Engineering Singapore and RS Components Sdn Bhd (Malaysia). Following insertion, all

306 thermocouples were connected to a datalogger to record the CCL temperatures at 4-second
307 intervals. The heat pad and the TDSL were placed directly on top of the CCL. A small
308 overburden stress of approximately 1.5 kPa was applied by placing metal weights on top of the
309 heat pad in order to ensure good contact with the TDSL. Southen, Rowe [15] reported that the
310 overburden stress has an insignificant effect on the desiccation of liners and moisture
311 redistribution. Therefore, the effect of a varying overburden stress on liner desiccation was not
312 analysed in this study. Moreover, a LCS was not included in order to be conservative, since the
313 presence of LCS above CCL reduces the heat flow to CCL due to the low thermal conductivity
314 of the LCS's gravel medium [36]. **Fig. 6(a)** provides a schematic diagram of the liner
315 configuration set up for the *base case*.

316 **3.4.3. Cooling case**

317 In the *cooling case*, a cooling pipe system that comprised a single four-pass module
318 embedded within a fine sand layer (referred to as *pipe sand layer* or *PSL*) was placed on top of
319 the CCL. **Figs. 6(b)** and **7** show the liner configuration of the *cooling case* and plan view of
320 the laboratory cooling pipe network, respectively. The cooling pipes were connected to a
321 SUNSUN HJ-1500 submersible water pump (immersed in a cool water supply tank) and a
322 cooling tank to form a closed loop. The submersible pump was used to pump water into the
323 entry pipe and the cooling tank was used to reduce the temperature of the heated water flowing
324 through the return pipe before it was directed back to the water supply tank. A scaling factor
325 of 10 was used for the PSL thickness, pipe diameter, pipe spacing and coolant flow rate. The
326 PSL thickness was simply assumed to be 0.35 m in the field in order to be conservative, since
327 the lower the sand layer thickness between the heated waste and the CCL, the higher the heat
328 flow to the CCL [38]. Having considered previous works conducted by [35]; and [36], the
329 (inner) pipe diameter and pipe spacing (between the entry and return pipes within a module) in
330 the field were assumed to be equivalent to 150 mm and 2.6 m, respectively.

Accordingly, an inner diameter of 15 mm and an intermodular pipe spacing of 260 mm were chosen for the laboratory pipe network. Moreover, the effect of doubling the coolant flow rate on the reduction of CCL temperature and desiccation were tested. The two flow rates chosen for the laboratory cooling pipe system were 0.75 m^3/h (Re = 21275) and 1.5 m^3/h (Re = 43857), both of which ensured turbulent flow conditions, since prior studies have shown that turbulent flow results in a higher heat extraction rate and a lower liner temperature [4, 66, 67]. When scaled up while preserving the Reynold's number, the laboratory flowrates of 0.75 m^3/h and 1.5 m^3/h correspond to approximately 7.5 m^3/h and 15 m^3/h in the field, respectively.

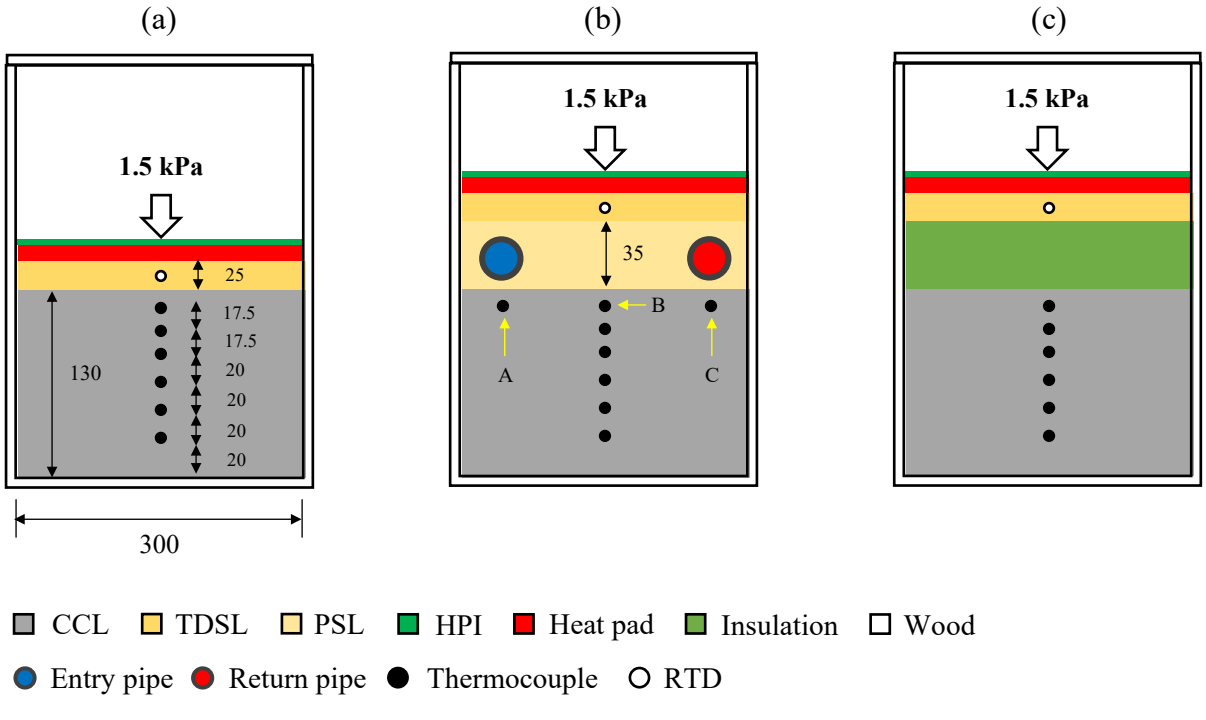

Fig. 6. Schematic diagrams of laboratory liner configurations for: (a) base case; (b) cooling case; (c) insulation case (all dimensions in mm)

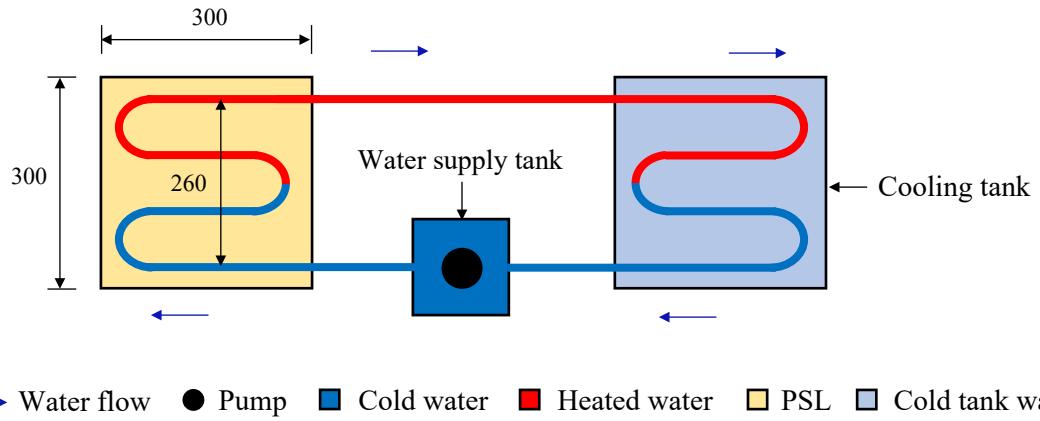

342

343 **Fig. 7.** Top view of laboratory cooling pipe network (all dimensions in mm)

344 ### 3.4.4. Insulation case

345 In the *insulation case*, the pipe array and sand layer were replaced with a rockwool
346 insulation layer above the CCL. Accordingly, the effect of varying thickness of the rockwool
347 insulation layer on the reduction of CCL temperature and desiccation was investigated through
348 three rockwool thicknesses of 20 mm, 35 mm and 50 mm. Since previous studies that utilized
349 rockwool for insulation within buildings showed that the utilization of a rockwool thickness
350 greater than approximately 50 mm either led to a decline or an insignificant rise in net energy
351 savings, the maximum rockwool thickness employed for the present study was limited to 50
352 mm [68-70].

353 ### 3.4.5. Operation of the test program

354 A wooden lid was placed on top of the wooden tank following assemblage of the
355 experimental setup to minimize heat transfer between the external environment and internal
356 contents of the tank during operation. The heat pad and datalogger were then switched on and
357 allowed to run continuously until the variation of temperature at various depths within the CCL
358 became stable over time. Once the temperature readings were observed to become relatively
359 stable, the experimental program was terminated. Subsequently, coring tubes were inserted into
360 the mid-region of the CCL and core samples were obtained via extrusion. The extruded core

samples were then sliced and the final gravimetric water content of each slice (located at a certain depth within the CCL) was determined [27].

4. Results and Discussion

4.1. Base case

4.1.1. Temporal variation of CCL temperature

During the *base case*, the CCL was subjected to constant elevated temperatures (CETs) of 70°C, 55°C and 40°C, respectively until the temperature distributions within the CCL stabilised over time. **Figs. 8(a-c)** shows the temporal variation of the soil temperature at different depths within the CCL's mid-region for all three CETs. It is clear from **Figs. 8(a-c)** that upon the application of heat (regardless of the magnitude), the CCL temperature increased dramatically within the first 12 to 18 hours and then gradually achieved a stabilised state over time. Since heat and moisture transport is known to be a *coupled* process, it was presumed that the temperature and moisture variation along the CCL depth stabilised concurrently. A similar observation was reported by Southen, Rowe [15] when they exposed a composite liner-subsoil profile to an elevated temperature, where significant temperature changes in the subsoil column were observed within the first 20 hours of heat application.

(a)

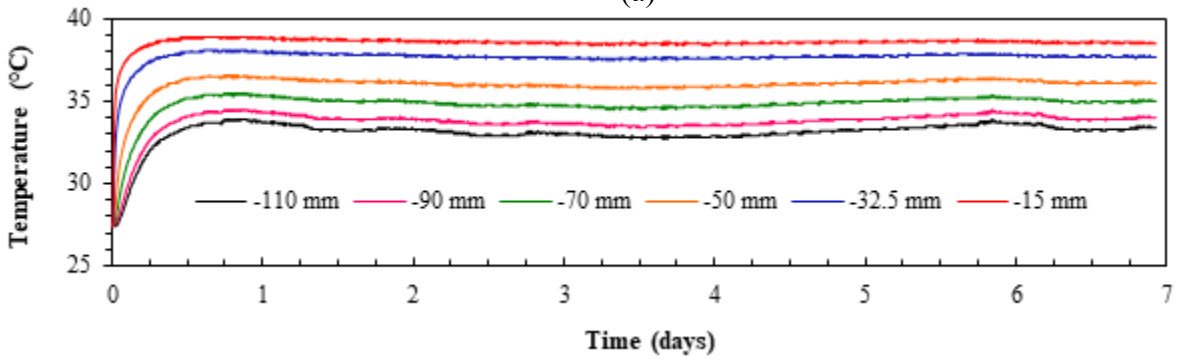

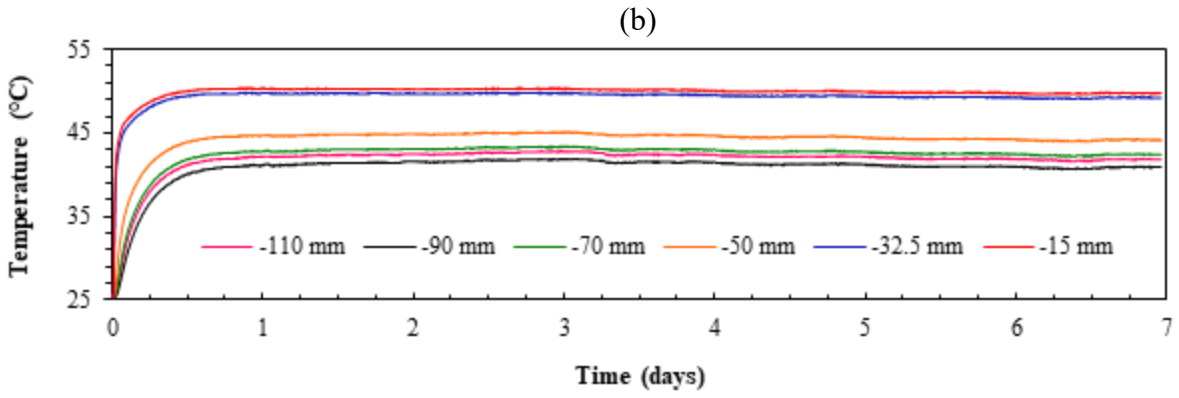

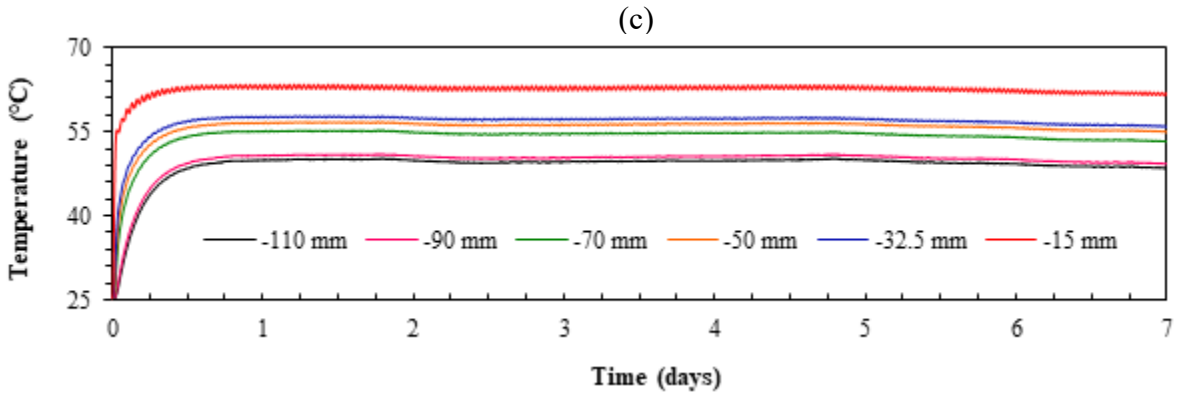

Fig. 8. Variation of temperature over time at different depths within the CCL when subjected to a constant elevated temperature (CETs) of (a) 40°C; (b) 55°C; (c) 70°C

4.1.2. CCL temperature profiles

Fig. 9 depicts the vertical profiles of the initial and final temperatures recorded along the depth of a CCL subjected to CETs of 70°C, 55°C and 40°C, respectively. The vertical profiles of the initial temperature (IT) and final temperature (FT) correspond to the temperature readings that were obtained along the depth of the CCL's mid-region before heat application and at the end of the experiment when the temperatures were found to stabilise, respectively. **Fig. 9** shows that all final thermal profiles were non-linear and the temperature reduced with increasing CCL depth regardless of the CET magnitude. In order to better analyse the thermal distribution within the CCL, spline interpolation was performed between the experimental data points (along the CCL depth) and *OneWay splines (OWS)* were fitted using the SRS1 Splines software add-in installed in Microsoft excel [71]. The OneWay spline is similar to the Cubic

spline but uses a parabolic fit internally for its interpolation and is more constrained. The fitted OW splines ensured continuity of the experimental results by filling the gaps between the experimental data points, which in turn enabled the calculation of constant elevated temperature attenuation percentages (CETAPs) along the CCL depth.

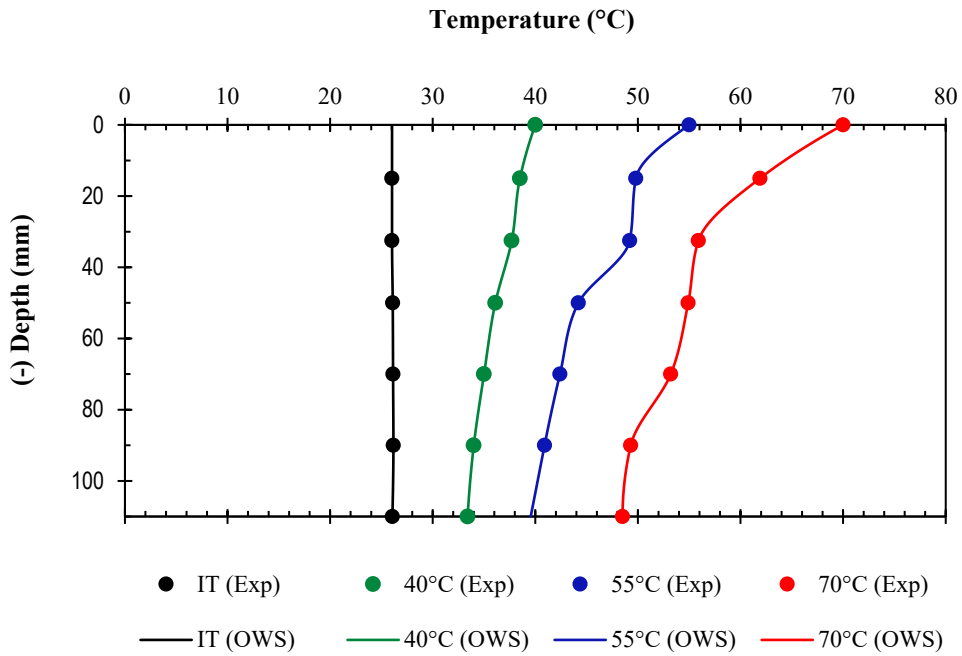

Fig. 9. Initial (IT) and final temperature (FT) variation along the depth of a CCL subjected to constant elevated temperatures (CETs) of 70°C, 55°C and 40°C

With the aid of OW spline interpolation, the CETAPs were calculated along the depth of the CCL's mid-region at intervals of 0.2 mm (for over 550 locations) using **Eq. (1)**, where T_{CET} and T_f refer to the applied CET and the FT at different depths along the CCL's mid-region, respectively. Accordingly, **Fig. 10** displays the calculated CETAPS along the CCL depth for all three CETs. It is evident from **Fig. 10** that as the CET magnitude increased, the CETAP increased as well. The CCL subjected to a CET of 70°C experienced a total temperature drop of approximately 30.7% at a depth of 110mm, while the CCLs subjected to CETs of 55°C and 40°C experienced temperature losses of 28.1% and 16.5%, respectively. Besides CETAP, the final temperature (FT) gradient along the CCL depth was also calculated

using **Eq. (2)**, where T_{f1}, T_{f2} and H refer to the FT at 0 mm depth, FT at -110 mm depth and the 110 mm height of the analyzed CCL region, respectively [13, 15, 65, 72]. Accordingly, the calculated vertical FT gradients for CETs of 70°C, 55°C and 40°C, were approximately 1.9°C/cm, 1.4°C/cm and 0.6°C/cm, respectively. The obtained values indicate that the vertical FT gradient (or the rate of CET attenuation) along the CCL depth rose with increasing CET.

$$CETAP\ (\%) = \frac{T_{CET} - T_f}{T_{CET}} \times 100 \qquad \textbf{Eq. (1)}$$

$$FT\ gradient\ (°C/cm) = \frac{T_{f1} - T_{f2}}{H} \qquad \textbf{Eq. (2)}$$

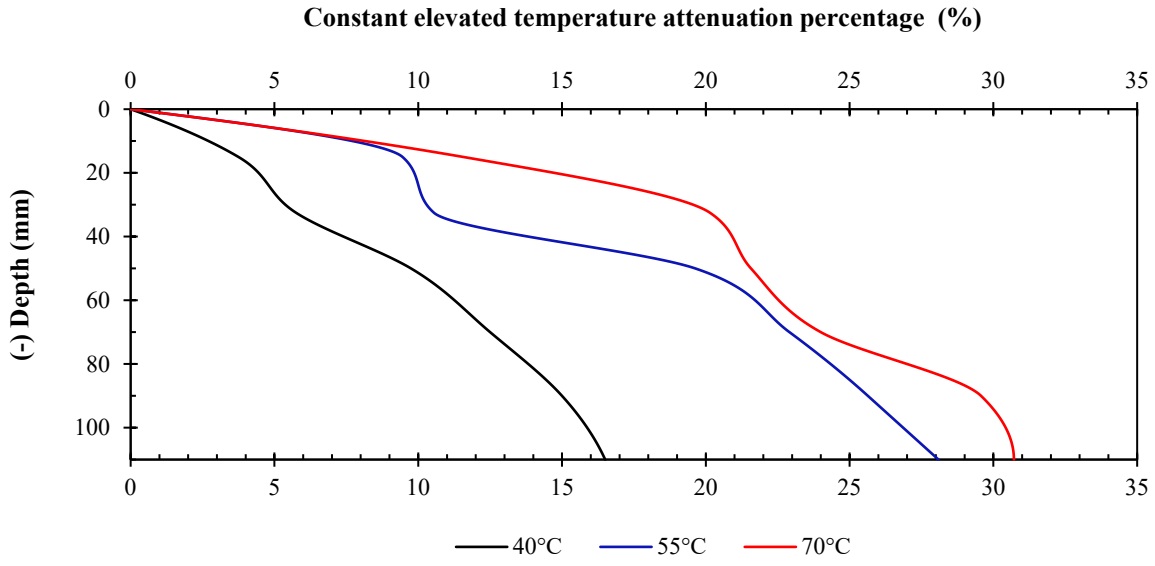

Fig. 10. Constant elevated temperature attenuation percentage (CETAP) along the depth of a CCL subjected to constant elevated temperatures (CETs) of 70°C, 55°C and 40°C

The nonlinear temperature attenuation observed in each FT profile was primarily governed by the water content reduction that occurred along the CCL depth upon exposure to CETs. Heat transport through soil occurs almost entirely via conduction. Heat transfer through convection is considered to be significant only under circumstances where a high flow rate water or air is present, while heat transfer through radiation is considered to be significant for only surface soils [73]. Heat flow through soil via conduction can be explained using *Fourier's*

law, expressed in **Eq. (3)** in one-dimensional form, where the Q, k, A, T, z and dT/dz refer to heat transfer rate, thermal conductivity, surface area normal to the direction of heat transfer, soil temperature, soil depth and vertical temperature gradient, respectively [74, 75]. Provided that the soil surface area A remains constant throughout the analyzed soil depth z, it is clear from **Eq. (3)** that the rate of heat transfer through the soil is directly proportional to both the soil's thermal conductivity and its vertical temperature gradient. Thermal conductivity of the soil matrix is heavily influenced by the thermal conductivity of its pore fluid(s). Since the pore fluid fills the voids within the soil matrix and functions as a bridge between soil particles, its thermal conductivity directly affects the magnitude of heat transfer between soil particles. Therefore, the higher the thermal conductivity of the pore fluid, the higher the rate of heat transfer between soil particles, and vice versa [31].

$$Q\ (J/s) = kA\frac{dT}{dz} \qquad \textbf{Eq. (3)}$$

In the present study, when a CET was applied to the CCL's top surface, the heat flow through the CCL would have induced evaporation of the liquid pore water and converted it into pore water vapour. Subsequently, the pore water vapour would have either (a) remained within the clay voids, or (b) diffused to cooler regions and enabled the voids it initially occupied to be replaced with air. Since the thermal conductivity values of water vapour and air are known to be significantly lower than that of liquid water [76, 77], the replacement of liquid pore water in clay voids with either pore water vapour or air would have significantly hindered the heat flow between clay particles. Accordingly, the evaporation of liquid pore water along the CCL depth would have led to reduced downward heat flow and consequently, attenuation of the applied CET along the CCL. Furthermore, a rise in the CET would have lead to an increased vertical temperature gradient and consequently, an increased rate of heat transfer along the CCL depth (according to **Eq. (3)**). This would have in turn led to an increased evaporation of

liquid pore water along the CCL depth (particularly in the uppermost portion) and ultimately an increased reduction of CET, i.e., an increased CETAP as clearly visible in **Fig. 10**.

4.1.3. CCL water content profiles

Figs. 11(a-c) portray the vertical profiles of the initial and final gravimetric water contents measured along the depth of the CCL subjected to CETs of 70°C, 55°C and 40°C, respectively. The vertical profiles of the initial water contents (IWC) and final water contents (FWC) correspond to the water contents measured along the depth of the CCL's mid-region prior to the application of heat and following termination of the experiment, respectively. As expected, **Figs. 11(a-c)** show that the application of heat led to a reduction of water content along the entire depth of the CCL. Moreover, the magnitude of water content reduction declined with increasing depth of the CCL. Similar to the case with thermal profiles, *OneWay* splines were fitted to the the experimental data points to ensure continuity along the CCL depth and enable the calculation of water content reduction percentage (WCRP) along the depth of the CCL's mid region when subjected to CETs of 70°C, 55°C and 40°C, respectively. The WCRP (with respect to the initial water contents) was calculated along the depth of the CCL's mid-region at intervals of 0.2 mm using **Eq. (4)**, where w_i and w_f refer to the initial and final water contents at different depths along the CCL's mid-region, respectively. Accordingly, **Fig. 12** depicts the calculated WCRPs along the CCL depth for the three CETs.

$$WCRP\ (\%) = \frac{w_f - w_i}{w_i} \times 100 \qquad \textbf{Eq. (4)}$$

$$FWC\ gradient\ (\%\ \text{per cm}) = \frac{w_{f1} - w_{f2}}{H} \qquad \textbf{Eq. (5)}$$

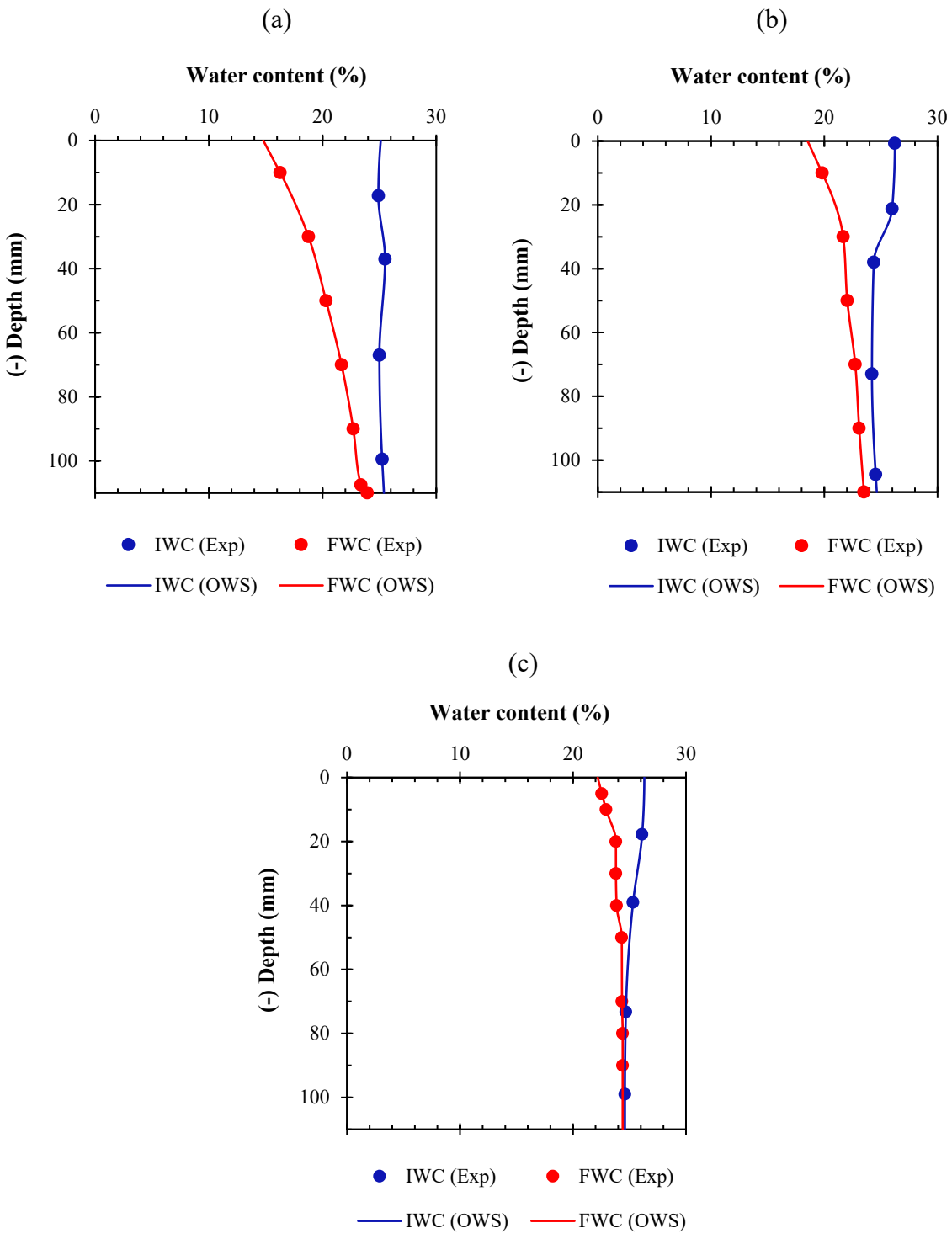

Fig. 11. Initial (IWC) and final water content (FWC) variation along the depth of a CCL subjected to constant elevated temperatures (CETs) of: (a) 70°C; (b) 55°C; (c) 40°C

Fig. 12 shows that the WCRP declined with increasing CCL depth for all CETs and the *rate* of water content reduction was generally higher in the uppermost region of the CCL for

all CETs. Moreover, the WCRP rose as the CET increased. The CCL that was subjected to a CET of 70°C suffered a maximum water content reduction of approximately 41.1% at the CCL top surface (where the highest heat was experienced), while the CCLs subjected to CETs of 55°C and 40°C experienced water content losses of 29.4% and 15.7% at the same location, respectively. The final water content (FWC) gradient formed along the CCL depth was calculated using **Eq. (5)**, where w_{f1}, w_{f1} and H refer to the FWC at -110 mm depth, FWC at 0 mm depth and the 110 mm height of the analyzed CCL region, respectively. Accordingly, the calculated vertical FWC gradients for CETs of 70°C, 55°C and 40°C, were 0.8% per cm, 0.5% per cm and 0.2% per cm, respectively. The obtained values indicate that the FWC gradient along the CCL depth rose as the CET increased.

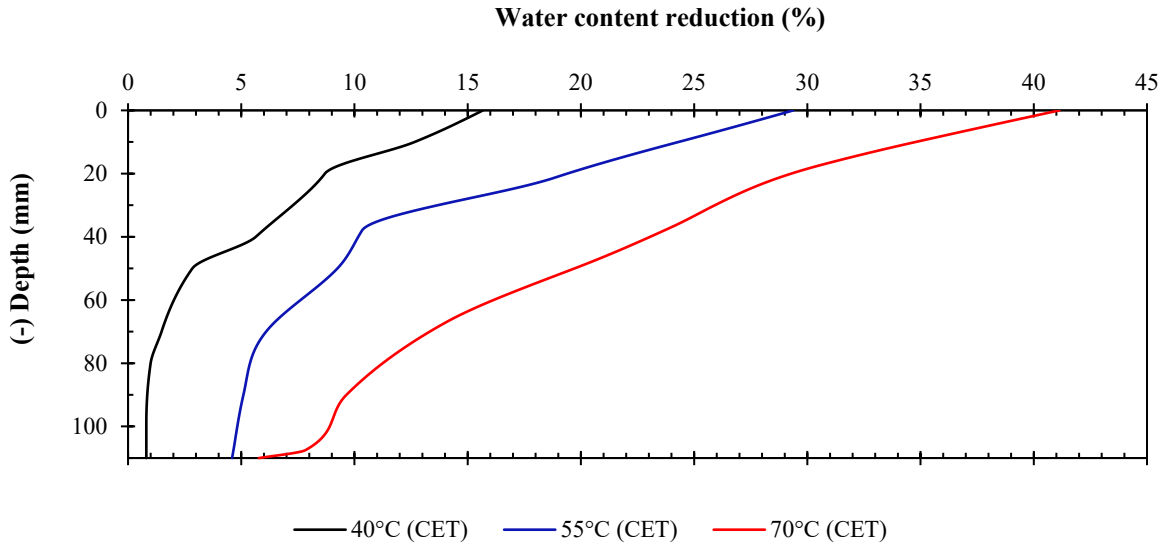

Fig. 12. Water content reduction percentage (WCRP) along the depth of a CCL subjected to constant elevated temperatures (CETs) of 70°C, 55°C and 40°C

The attenuation of WCRP with increasing CCL depth could be explained by the reduced downward heat flow through the CCL. As the magnitude of heat flowing through the CCL reduced with increasing depth, the magnitude of liquid pore water that evaporated as a result of the heat would have also decreased, which would have in turn lessened the reduction of water content with increasing CCL depth. This would also explain why the rate of water content

reduction was significantly greater in the uppermost region of the CCL where the heat flow was higher. Moreover, an increase in the magnitude of CET applied on the CCL surface would have evidently led to a corresponding increase in the magnitude of downward heat flow through the CCL. Increased downward heat flow would have caused a rise in liquid pore water evaporation and led to an increased water content reduction along the CCL. This would explain the rise in WCRP observed with increasing CET.

4.2. Insulation case

4.2.1. CCL temperature profiles

Figs. 13(a) and **(b)** depict the final temperature profiles measured along the depth of a CCL subjected to constant elevated temperatures (CETs) of 40°C and 70°C, respectively, in the presence of 0 mm, 20 mm, 35 mm and 50 mm thick rockwool layers. Similar to the *base case*, OneWay (OW) splines were fitted to experimental data points along the CCL depth. Final temperature (FT) profiles measured during the *insulation case* show that similar to the *base case* results, the applied CET reduced with increasing CCL depth regardless of the CET or rockwool layer thickness. This observation is attributed to the coupled heat-moisture transport theory suggested previously in *section 4.1.2.* More importantly, **Figs. 13(a)** and **(b)** show that the FT profiles measured along the CCL depth reduced as the applied rockwool thickness increased. Rockwool possesses a high thermal resistance since it contains a large quantity of microscopic dead air cells. Heat transfer occurs via three modes, viz. conduction, convection and radiation. Since air is a poor thermal conductor, the heat transfer through rockwool via conduction is reduced substantially. Moreover, since the air particles are essentially trapped inside tiny pockets within rockwool, their movement is significantly restricted, which results in reduced heat transfer via convection. Finally, the presence of tiny dead air cells also causes the radiation paths to break up into small distance segments so that the long-wave infrared radiation is absorbed and/or scattered by rockwool, which ultimately

leads to the reduction of heat transfer via radiation as well [78]. Therefore, in general, rockwool retards heat flow that occurs through all three heat transfer modes.

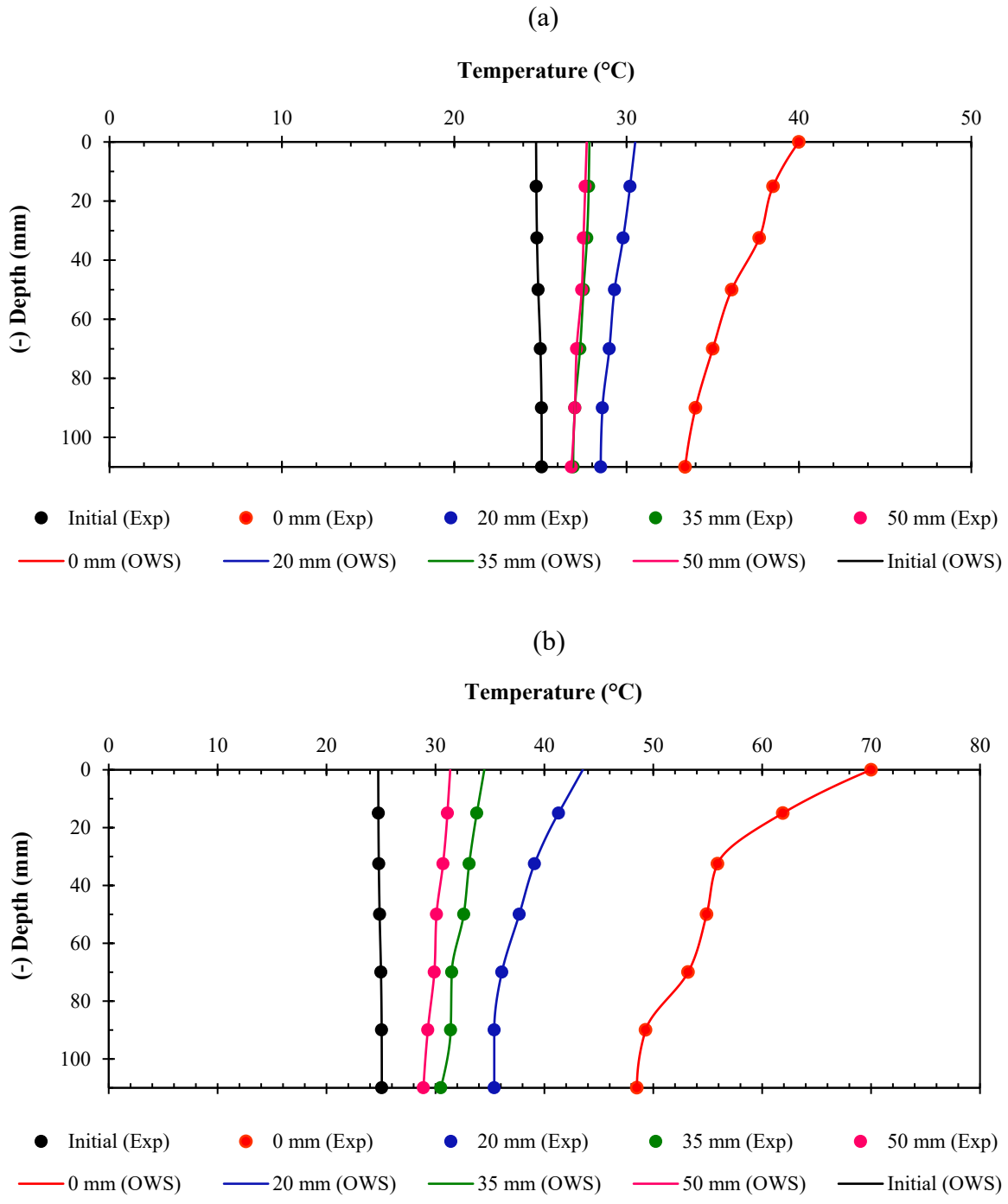

Fig. 13. Final temperature variation along CCL depth for different rockwool thicknesses: (a) 40°C CET; (b) 70°C CET

Fig. 13(a) shows that in the face of 40°C CET, all three rockwool thicknesses ensured that the CCL temperature remained below 35°C, which is generally considered the elevated temperature limit for the liner, since temperatures above 35°C possess the ability to adversely affect the liner's performance [8, 9, 13, 36, 79, 80]. In the face of 70°C however, only 35 and 50 mm rockwool thicknesses maintained the CCL temperature below 35°C, as depicted in **Fig. 13(b)**. In order to further analyse the effectiveness of rockwool application on CCL temperature reduction, the FT attenuation percentages (FTAPs) were calculated for different rockwool thicknesses using **Eq. (6)**, where the terms, T_{bc} and T_{ic} refer to the *base case* FT and *insulation case* FT, respectively. The FTAP values indicate the percentage by which the *base case* FT profile reduced when a specific rockwool thickness was applied on top of the CCL, respectively. **Fig. 14(a)** displays the calculated FTAPs for varying rockwool thicknesses along the depth of a CCL subjected to a 40°C CET. It can be seen from **Fig. 14(a)** that the introduction of a 20 mm rockwool thickness immediately led to a significant reduction of the *base case* FT by 14.7-23.8%. However, while a rise in rockwool thickness led to a continuous increase in the FTAP, the *rate* at which the FTAP rose, dropped steeply as the rockwool thickness increased.

$$FTAP\ (\%) = \frac{T_{bc} - T_{ic}}{T_{bc}} \times 100 \qquad \textbf{Eq. (6)}$$

For example, the computed FTAP growth rate for rockwool thickness increment from 0 to 20 mm was 1.2% per mm, whereas that calculated for rockwool thickness increment from 35 to 50 mm was 0.03% per mm. From these results, it is perceived that for an applied CET of 40°C, increasing the insulation thickness was truly effective only until a certain thickness was reached (which in this case, was 35 mm), following which, the additional heat flow retardation achieved by further increasing the rockwool thickness was negligible. Taking into consideration the effectiveness of the three thicknesses in reducing CCL temperature and their individual material/installation costs (which are major factors in large scale applications), the

authors recommend that a 20 mm rockwool insulation thickness be employed in MSW landfills where the ETs encountered by CCL are equal to or lower than 40°C, in order to achieve a satisfactory temperature reduction at a reasonable cost.

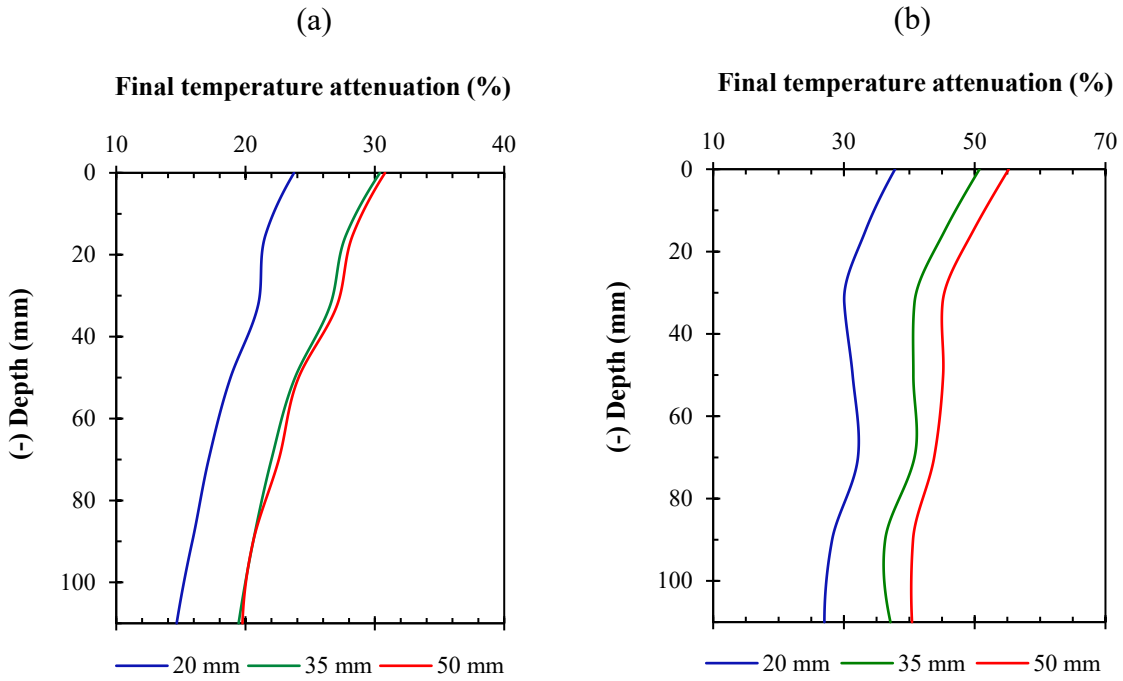

Fig. 14. Final temperature attenuation percentage (FTAP) variation along CCL depth for different rockwool thicknesses: (a) 40°C CET; (b) 70°C CET

Meanwhile, **Fig. 14(b)** portrays the calculated FTAPs along the depth of a CCL subjected to a 70°C CET for varying rockwool thicknesses. Similar to the 40°C CET case, while rockwool thickness increments led to a progressive reduction of CCL temperature, the temperature reduction rate reduced with increasing rockwool thickness. However, unlike in the case of 40°C, the additional temperature reduction achieved by increasing the thickness from 35 mm to 50 mm was still significant. As per the second law of thermodynamics, heat flows from hot to cold regions. The higher the temperature difference between the hot and cold regions (i.e., temperature gradient), the higher the rate of heat transfer (as expressed in **Eq. (3)**). When 70°C ET was applied above the CCL by the heat source, the temperature difference between the initially cool CCL bottom and the heat source was much higher than in the case of

556 40°C CET application. As a result, the heat flow triggered by 70°C CET was so high that even
557 after the application of 35 mm thickness, a significant heat flow was still present for the 50 mm
558 thickness to retard. Nevertheless, the 35 mm rockwool thickness was still able to attenuate the
559 CCL temperature from a high range of 48.5-70°C to a low range of 30.5-34.5°C. This
560 corresponded to a FTAP range of 37.1-50.7%. Accordingly, the authors recommend that a 35
561 mm rockwool thickness be deployed in MSW landfills that encounter ETs equal to or lower
562 than 70°C.

563 **4.2.2. CCL water content profiles**

564 **Figs. 15(a)** and **(b)** depict the final gravimetric water content profiles measured along
565 the depth of a CCL subjected to CETs of 40°C and 70°C, respectively, in the presence of
566 different rockwool thicknesses. It can be observed that the FWC profiles generally decreased
567 along the CCL depth regardless of the CET or insulation thickness. This observation is
568 attributed to the reduced downward heat flow along the CCL depth, explained in *section 4.1.3*.
569 In order to analyse the effect of rockwool insulation on the desiccation reduction of the CCL,
570 *water content growth percentages (WCGPs)* were calculated using **Eq. (7)**, where the terms
571 w_{bc} and w_{ic} refer to the FWCs of *base case* and *insulation case* experiments, respectively. The
572 WCGP values indicate the percentage by which the *base case* FWC profile increased when a
573 specific insulation thickness was applied on top of the CCL. **Fig. 16(a)** portrays the variation
574 of WCGPs calculated for different rockwool thicknesses along the depth of a CCL subjected
575 to a 40°C CET. From both **Figs. 15(a)** and **16(a)**, it can be observed that as the insulation
576 thickness increased, the FWC generally rose as well (particularly within the CCL's upper
577 region).

$$Water\ content\ growth\ percentage\ (\%) = \frac{w_{ic} - w_{bc}}{w_{bc}} \times 100 \qquad \textbf{Eq. (7)}$$

578 **Fig. 16(b)** depicts the variation of WCGPs calculated for different rockwool
579 thicknesses along the depth of a CCL subjected to a 70°C CET. Unlike in the case of 40°C
580 CET, an apparent rise in the FWC throughout the CCL depth following rockwool application
581 can be observed in **Figs. 15(b)** and **16(b)**. Since the desiccation that CCL experienced
582 throughout its depth in the face of 70°C CET was much higher than what it experienced when
583 exposed to 40°C CET during the base phase, the desiccation reduction along the CCL depth
584 when exposed to 70°C CET was more apparent in the presence of insulation. From **Figs. 15(b)**
585 and **16(b)**, it can also be observed that the FWC along the CCL depth generally rose with
586 increasing insulation thickness, especially in the CCL's uppermost region. Moreover, the
587 magnitude of desiccation reduction achieved by each insulation thickness reduced with
588 increasing CCL depth. This is because the desiccation magnitude suffered by the CCL during
589 the 70°C CET *base case* experiment reduced with increasing CCL depth.

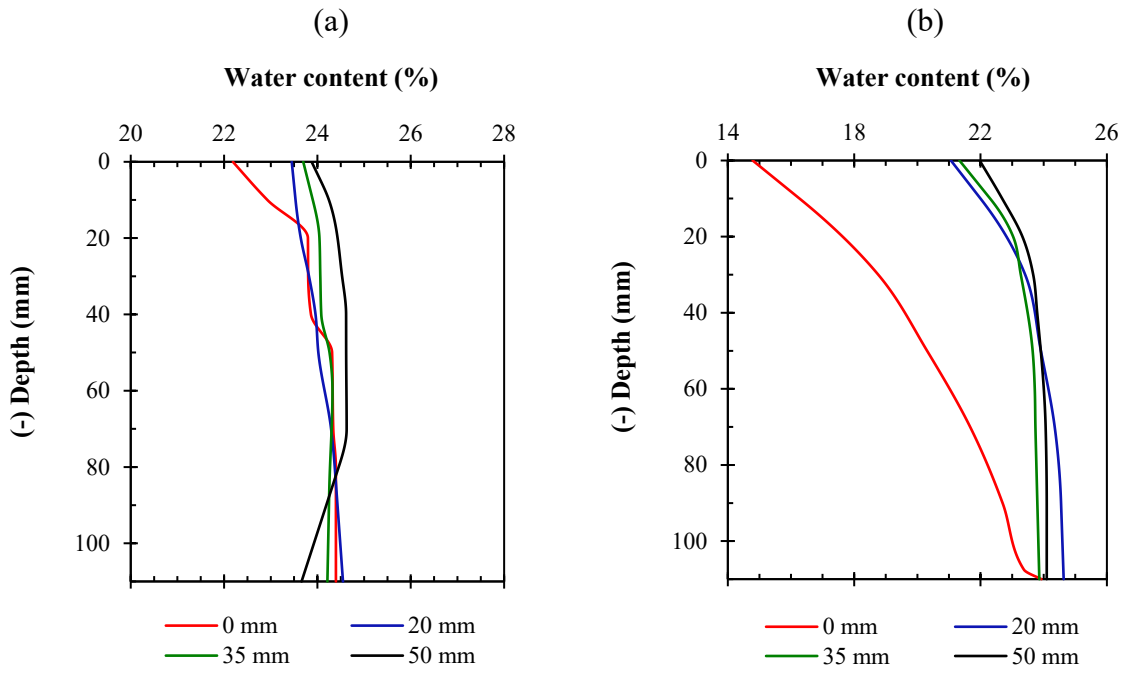

590 **Fig. 15.** Final water content profiles along CCL depth for different rockwool thicknesses: (a)
591 40°C CET; (b) 70°C CET

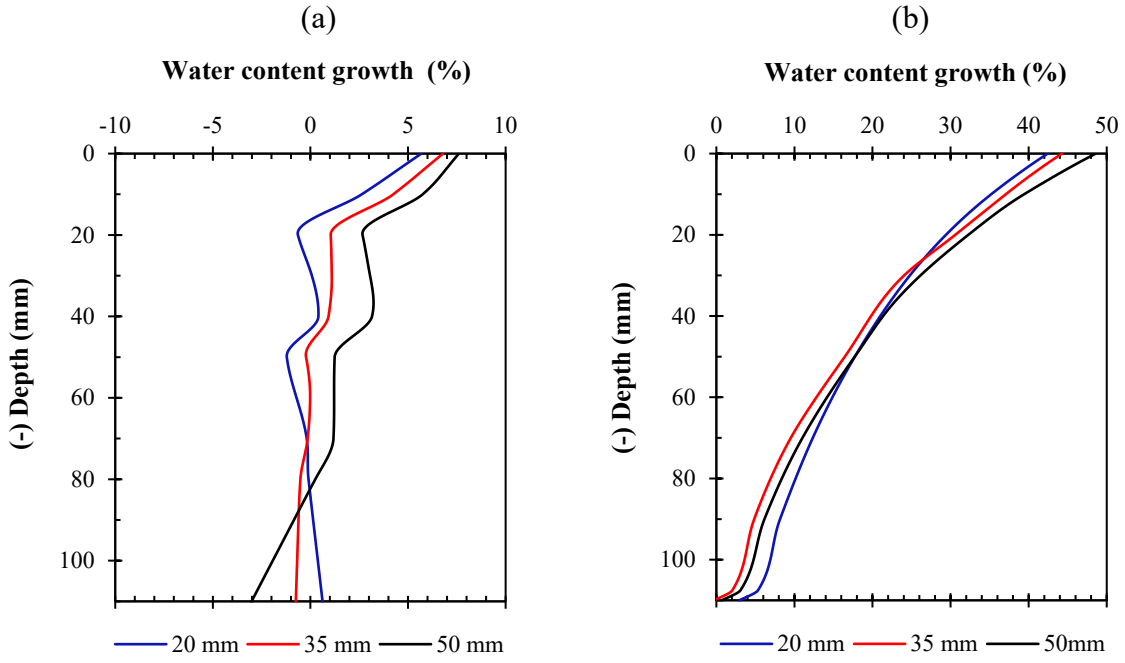

592 **Fig. 16.** Water content growth percentage variation along CCL depth for different rockwool
593 thicknesses: (a) 40°C CET; (b) 70°C CET

594 **4.3. Cooling case**

595 **4.3.1. CCL temperature profiles**

596 **4.3.1.1. Effect of cooling pipes**

597 **Figs. 17(a)** and **(b)** depict the final temperature profiles measured along the depth of a
598 CCL subjected to constant elevated temperatures (CETs) of 40°C and 70°C, respectively, in
599 the presence of galvanized steel cooling pipes. Similar to the *base* and *insulation cases*,
600 OneWay (OW) splines were fitted to experimental data points along the CCL depth. Final
601 temperature (FT) profiles measured during the *cooling case* show that, similar to the *base case*
602 results, the applied CET reduced with increasing CCL depth regardless of the CET or coolant
603 flowrate employed applied. This observation is attributed to the coupled heat-moisture
604 transport theory suggested previously in *section 4.1.2.* More importantly, **Figs. 17(a)** and **(b)**
605 show that the FT profiles measured along the CCL depth reduced when cooling pipes were
606 introduced, regardless of the CET that was applied. This observation is attributed to the heat
607 exchange that would have occurred between the coolant, cooling pipe wall and the sand layer

608 that surrounded the cooling pipe (i.e., the PSL). Heat is known to flow from hot to cold regions,
609 as described by the second law of thermodynamics. When a constant elevated temperature
610 (CET) was applied to the top surface of the PSL, the heat would have flowed downwards
611 through the fine sand grains via conduction towards the CCL and the cooling pipes would have
612 intersected the heat flow before it reached the CCL. Subsequently, the heat would have
613 transferred from the sand grains to the pipe wall via conduction and from the pipe wall to the
614 coolant via convection.

615 Convection that occurs in a fluid when in motion, is classified as natural and forced
616 based on the motion's initiation mechanism. Simply stated, convection that occurs in a fluid
617 that is *forced* to flow by external means, is termed forced convection, whereas convection that
618 occurs in a fluid whose motion is caused via *natural* means (such as buoyancy effect), is termed
619 natural convection. Accordingly, since the coolant was pumped into the pipe network via a
620 water pump in the present study, it is presumed that the heat transfer from the pipe wall to the
621 coolant would have occurred via forced convection. The transfer of a significant magnitude of
622 heat from the PSL to the coolant would have led to a reduced heat flow towards the CCL. This
623 would have ultimately led to the formation of a final temperature profile along the CCL depth
624 that was lower than that formed in the absence of cooling pipes (i.e., during the *base case*).

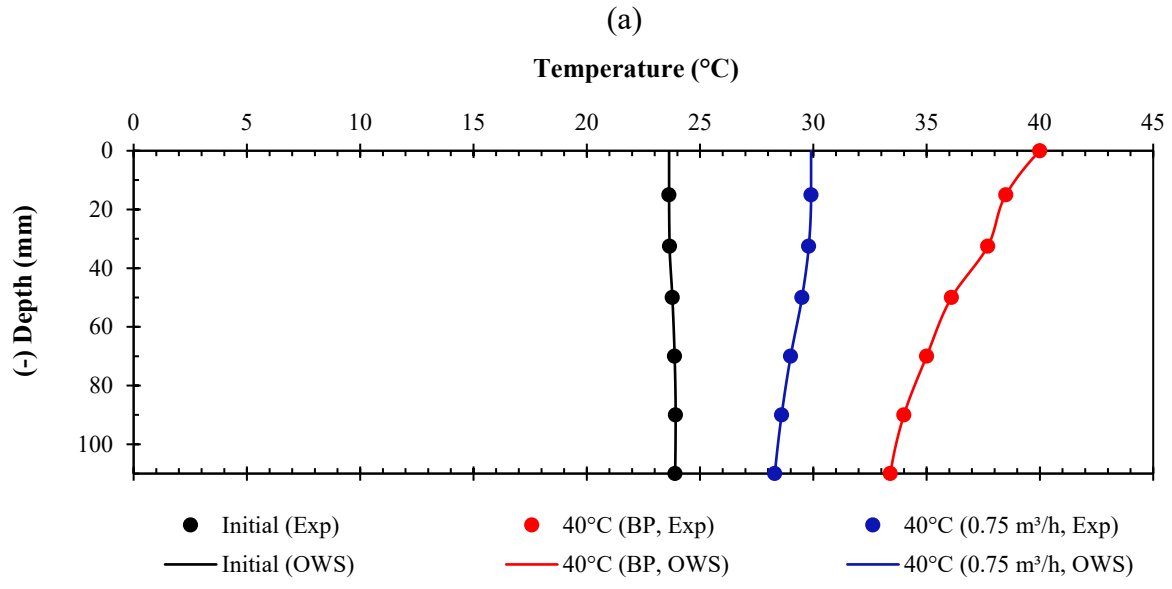

625

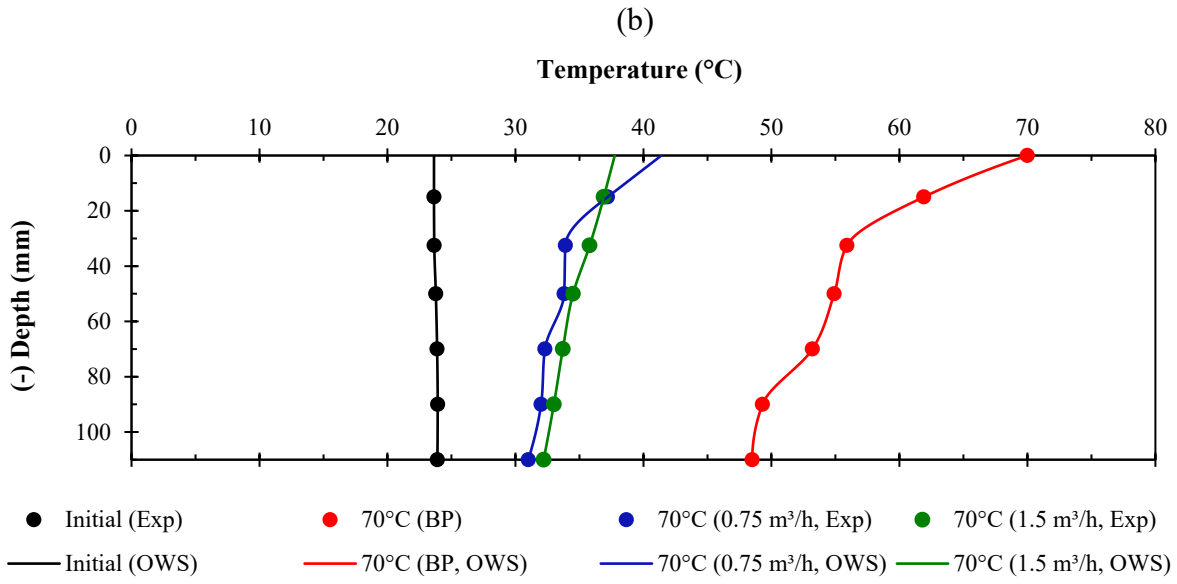

626

627 **Fig. 17.** Final temperature variation along CCL depth in the absence and presence of cooling

628 pipes: (a) 40°C CET; (b) 70°C CET

629 In order to further analyse the effectiveness of cooling pipe utilization on CCL

630 temperature reduction, the FT attenuation percentages (FTAPs) were calculated using **Eq. (8)**

631 where the terms, T_{bc}, T_{cc}, refer to the *base case* FT and *cooling case* FT, respectively. The

632 FTAPs calculated along the CCL depth denote the percentages by which the *base case* FT

633 profile along the CCL depth reduced when cooling pipes were introduced.

$$FTAP\ (\%) = \frac{T_{bc} - T_{cc}}{T_{bc}} \times 100 \qquad \textbf{Eq. (8)}$$

634 **Fig. 18** portray the variation of calculated FTAPs along the depth of a CCL subjected

635 to CETs of 40°C and 70°C in the presence of cooling pipes. From **Fig. 18**, it is apparent that

636 under a CET of 40°C, the introduction of cooling pipes (with a flow rate of 0.75 m^3/h) led to a

637 significant reduction of the *base case* FT by 15.3-25.3%. The maximum temperature recorded

638 along the depth of the CCL for the 0.75 m^3/h GS 40°C CET experiment was 29.9°C, which

639 occurred at the CCL's top surface. Since this temperature was lower than the adverse 35°C

640 elevated liner temperature limit, the proposed cooling pipe system in its current state was

deemed appropriate to be employed in MSW landfills that encounter ETs equal to or lower than 40°C. Meanwhile, the FTAP values calculated for the 0.75 m^3/h GS 70°C CET experiments were of the range 36.1-40.9%. From **Figs. 17(b)** and **18**, it is clear that the cooling pipes (regardless of the flow rate employed) struggled to attenuate the heat that flowed towards the CCL when a CET of 70°C was applied. This is because the application of a 70°C CET triggered an intense downward heat flow due to the high temperature difference that existed between the heat source and the cool CCL bottom at the time of heat application. The maximum temperatures recorded along the depth of the CCL's mid region for the 0.75 m^3/h and 1.5 m^3/h GS 70°C CET experiments were 41.4°C and 37.8°C, respectively, both of which are higher than the adverse 35°C elevated liner temperature limit adopted in the present study.

Accordingly, the proposed cooling pipe system in its present state is not recommended to be deployed in MSW landfills that experience ETs close to 70°C, without economical adjustments being made to enhance the heat exchange efficiency that the cooling pipe system currently possesses. A few recommended adjustments include reducing the pipe spacing, increasing the pipe diameter, or even changing the medium surrounding the pipes from pure fine sand to materials with higher thermal conductivities such as mixtures of lime, concrete, sand and cement [4, 36, 67, 79]. **Fig. 19** displays the FTs measured at three specific points located 15 mm below the CCL's top surface for the 0.75 m^3/h GS experiments. The three points, as shown in **Fig. 6**, were located below the entry pipe (point-A), below the centre of the PSL (point-B) and below the return pipe (point-C), respectively. From **Fig. 19** it is apparent that for the 40°C CET experiment, the temperature difference between the three measured locations was minimal, most likely due to the low heat flow associated with the applied 40°C temperature.

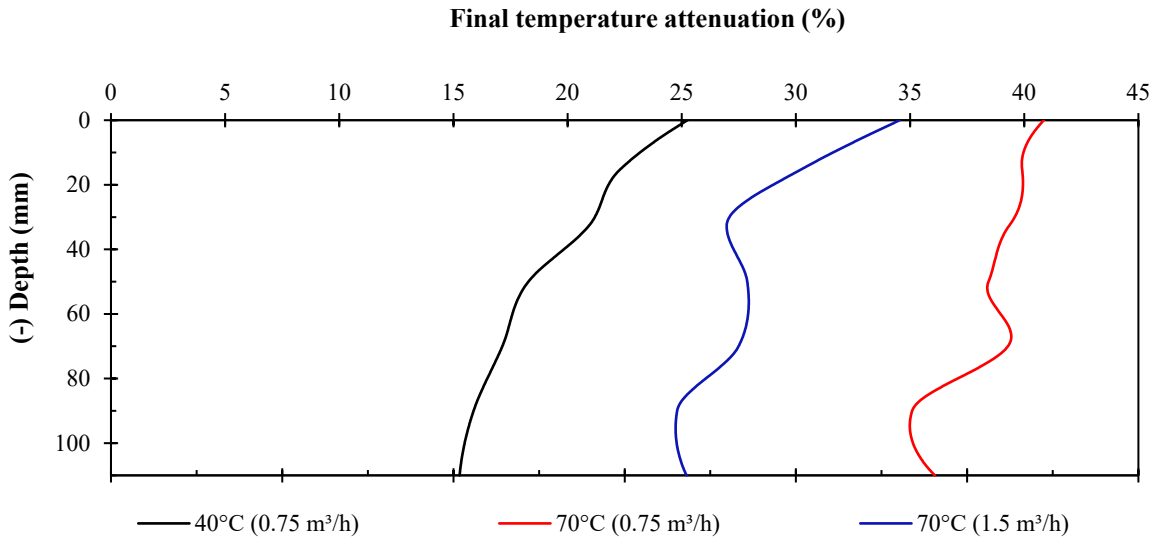

664

665 **Fig. 18.** Final temperature attenuation percentage (FTAP) variation along CCL depth in the

666 presence of cooling pipes

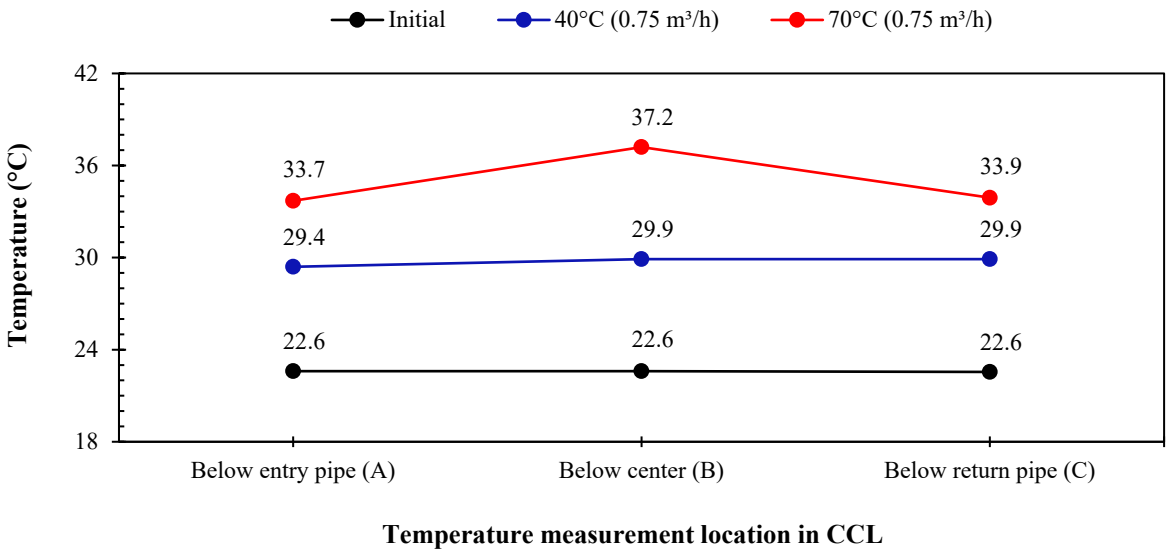

667

668 **Fig. 19.** Final temperature variation along the horizontal distance of a CCL subjected to

669 constant elevated temperatures of 40°C and 70°C in the presence of cooling pipes

670 On the contrary, a clear temperature pattern is noticed for the 70°C CET experiment.

671 The CCL temperature measured under the inlet and outlet were lower than that measured in

672 the centre region. This is due to the absence of any cooling pipes in the immediate vicinity of

673 the CCL's centre region. Moreover, for both 40°C and 70°C GS experiments, the CCL

674 temperature measured under the inlet was slightly lower than that measured under the outlet.

675 The coolant temperature would have been lower in the entry pipe than in the return pipe, since
676 the coolant would have absorbed a certain amount of heat from the PSL and become warm by
677 the time it reached the return pipe. Accordingly, the temperature difference between the PSL
678 and the coolant would have been higher in the entry pipe than in the return pipe. As a result,
679 the heat exchange rate would have been higher in the entry pipe than in the return pipe, which
680 would have resulted in the CCL located region underneath the entry pipe experiencing a higher
681 cooling than that located underneath the return pipe [79].

682 **4.3.1.2. Effect of coolant flow rate**

683 In addition to investigating the general reduction of CCL temperature in the presence
684 of cooling pipes, the effect of doubling the coolant flow rate (under turbulent conditions) on
685 CCL temperature reduction was also examined in the present study. This was because
686 according to the energy balance relationship generally used for steady-flow systems, the fluid
687 flow rate is proportional to the heat transfer rate to or from the fluid. Therefore, an increase in
688 fluid flow rate would lead to an increase in the net heat transfer rate between the cooling pipes
689 and the surrounding sand medium, which would in turn reduce CCL temperature. The energy
690 balance relationship is expressed in **Eq. (9)**, where the terms $\dot{Q}$, $\dot{m}$, c_p, T_i and T_e refer to heat
691 transfer rate (to or from the fluid), mass flow rate, specific heat, mean fluid temperature at the
692 inlet and mean fluid temperature at the exit of the tube, respectively [66].

$$\dot{Q}\ (W) = \dot{m} \times c_p(T_e - T_i) \qquad \textbf{Eq. (9)}$$

693 Interestingly however, it can be observed from **Figs. 17(a)** and **(b)** that the FT profiles
694 obtained for 0.75 m^3/h and 1.5 m^3/h flow rates were very similar to each other. This observation
695 is confirmed by **Fig. 18** which shows that doubling the flow rate merely increased the FTAP
696 range by 2.5-5.2%. Even the trivial reduction of CCL temperature that was achieved by
697 doubling the flow rate was limited to the uppermost 16 mm of the CCL. This indicates that

doubling the flowrate under turbulence conditions did not have a significant influence on CCL temperature reduction or more specifically, the net heat transfer rate. In general, when the velocity (or flow rate) of a fluid (i.e., the coolant in this case) is increased during heat exchange, the warm and cool masses of the fluid are brought into contact with each other more frequently, as a result of which heat is transferred via conduction at a greater number of sites within the fluid and the overall heat transfer rate across the fluid is increased. Essentially, the higher the fluid velocity (or flow rate), the higher the heat transfer rate. Accordingly, the rate of heat transfer across a fluid is known to rise significantly as it transitions from laminar to turbulent flow conditions (i.e., Re > 4000). This is because, unlike in the case of laminar flow conditions where thermal energy is transferred across streamlines via molecular diffusion, the thermal energy under turbulent flow conditions, is transported across the fluid much more rapidly by twirling eddies present in the flow which results in an increased rate of heat transfer. However, the rate of heat transfer is known to achieve a maximum limit when the flow reaches *fully* turbulent conditions, which corresponds to Reynolds number greater than 10,000 in most practical situations [66].

In the present study, the Reynolds numbers calculated for the two laboratory flowrates of 0.75 m^3/h and 1.5 m^3/h were 21275 and 43857, respectively. Based on the calculated Reynold numbers, it can be presumed that under a flow rate 0.75 m^3/h, the coolant flow (within the laboratory pipe network) would have already reached fully turbulent conditions, where the rate of heat transfer between the PSL and the cooling pipe would have most likely already reached its maximum limit. Therefore, increasing the coolant flow rate further would have led to an insignificant change in the rate of heat transfer and final temperature profile formed along the CCL depth. The same theory would apply to the proposed field-scale cooling pipe system as well since the Reynold's number is preserved when the laboratory flow rates are scaled up. It can thus be concluded that flow rate variation would have an insignificant effect on CCL

723 temperature reduction as long as the flow rate employed ensures fully turbulent conditions
724 within the pipe network.

725 **4.3.2. CCL water content profiles**

726 **Fig. 20(a)** depicts the final gravimetric water content profiles measured along the depth
727 of a CCL subjected to CETs of 40°C and 70°C in the presence of cooling pipes. It can be
728 observed that the FWC profiles generally decreased along the CCL depth regardless of the CET
729 or coolant flow rate. This observation is attributed to the reduced downward heat flow along
730 the CCL depth, explained in *section 4.1.3*. In order to analyse the effect of cooling pipes on the
731 desiccation reduction of the CCL, *water content growth percentages (WCGPs)* were calculated
732 using **Eq. (10)**, where the terms w_{bc} and w_{cc} referred to the FWCs of *base case* and *cooling*
733 *case* experiments, respectively. WCGP values indicate the percentage by which the *base case*
734 final WC profile along the CCL depth increased when cooling pipes were employed. **Fig. 20(b)**
735 shows the variation of calculated WCGPs along the depth of a CCL subjected to CETs of 40°C
736 and 70°C in the presence of cooling pipes. It is evident from **Figs. 20(a)** and **Fig. 20(b)** that
737 regardless of the CET applied, the final water contents measured along the CCL depth were
738 generally higher in the presence of cooling pipes than in the absence. This is attributed to the
739 temperature reduction of the CCL achieved by the heat extraction of cooling pipes.

$$Water\ content\ growth\ percentage\ (\%) = \frac{w_{cc} - w_{bc}}{w_{bc}} \times 100 \qquad \textbf{Eq. (10)}$$

740 It can be observed that for the 40°C CET, only the uppermost region of the CCL
741 experienced a rise in the *base case* FWC when cooling pipes were introduced, whereas a
742 significant rise in *base case* FWC was observed throughout the entire depth of the CCL for the
743 70°C CET (regardless of the flow rate employed). This was because the heat flow triggered by
744 the application of 70°C CET during the *base case* caused the CCL to experience desiccation
745 consistently throughout its entire 110 mm depth, unlike in the case of 40°C CET, where the

CCL's desiccation was limited to its uppermost region (as shown in **Fig. 11(c)**). Finally, **Figs. 20(a)** and **(b)** show that doubling of flow rate led to an insignificant rise in the *base case* FWC measured along the CCL depth in general. This is expected since it was observed in *section 4.3.1.2* that increasing the flow rate under fully turbulent conditions had an insignificant effect on CCL temperature reduction.

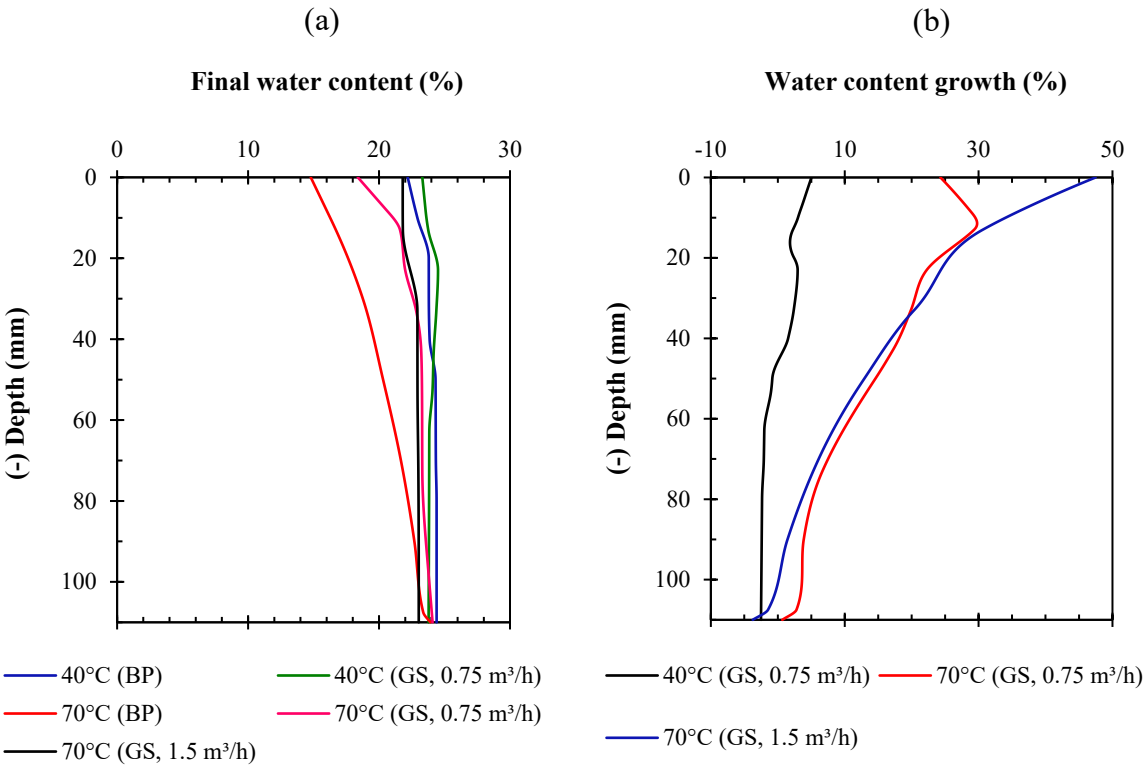

Fig. 20. (a) Final water content profiles along CCL depth in the presence of cooling pipes; (b) water content growth percentage along CCL depth in the presence of cooling pipes

5. Conclusion

The present study examined the variation of temperature-moisture profiles along the depth of a compacted clay liner (CCL) exposed to constant elevated waste temperatures (CETs) of the range 40°C-70°C in the absence and presence of two heat reduction techniques, viz. cooling pipes and rockwool insulation. Following analysis of the results obtained in this study, the following conclusions were drawn:

1. In the absence of any heat reduction techniques (i.e., in the *base case*), application of CETs led to an augmentation of temperature and reduction of water content along the entire depth of the CCL. The rise in temperature and reduction of water content along the CCL depth increased as the applied CET rose.
2. Introduction of rockwool insulation (in the *insulation case*) led to significant temperature reductions along the CCL depth under CETs of 40°C and 70°C. However, while rockwool thickness increments led to a progressive reduction of CCL temperature, the rate of temperature reduction attenuated with increasing thickness.
3. Introduction of rockwool insulation led to a significant reduction of the desiccation experienced by the CCL exposed to CETs of 40°C and 70°C. Desiccation of the CCL generally reduced as the insulation thickness increased.
4. Rockwool thicknesses of 20 mm and 35 mm were recommended to be employed for liner insulation in MSW landfills that encounter temperatures near 40°C and 70°C, respectively.The recommended thicknesses were the minimum thicknesses (from those tested) that were found to be sufficient to maintain the CCL's temperature below the 35°C elevated temperature limit, above which temperatures can adversely affect the liner's performance.
5. Introduction of cooling pipes (in the *cooling case*) led to significant reductions in temperature rise and desiccation along the CCL depth under CETs of 40°C and 70°C. The CCL region located underneath the entry pipe carrying cool water, experienced a higher cooling than that located underneath the return pipe carrying warm water.
6. Increasing the flowrate under fully turbulent conditions (Re > 10,000) did not have a significant influence on the reduction of CCL temperature and desiccation.
7. The proposed cooling pipe system in its current state was deemed appropriate to be employed in MSW landfills that encounter temperatures close to 40°C, but was not

recommended to be employed in those that encounter temperatures close to 70°C without economical adjustments being made to enhance the system's current heat exchange efficiency. This was because the maximum CCL temperatures recorded for the 70°C CET cooling pipe experiments exceeded the adverse 35°C elevated liner temperature limit adopted in the present study.

In general, the two proposed heat reduction techniques were found to be effective in successfully reducing the temperature rise and desiccation experienced by a CCL that is subjected to elevated temperatures in MSW landfills.

6. Credit author statement

Vihan Jayawardane: Conceptualization, Methodology, Experimentation, Results analysis; Writing - Original Draft

Vivi Anggraini: Writing - Review & Editing, Supervision, Funding

Manh-Vu Tran: Methodology, Supervision

Mehdi Mirzababaei: Results analysis, Writing - Review & Editing, Supervision

Agusril Syamsir: Funding

7. Declaration of Competing Interest

The authors declare that they have no known competing financial interests or personal relationships that could have inappropriately influenced the work reported in this paper

8. Acknowledgement

Financial support for this study is provided by the Ministry of Higher Education in Malaysia with grant number FRGS/1/2021/TK02/MUSM/03/1. This support is gratefully acknowledged.

9. Data availability

All data generated or analysed during this study are included in this published article.

10. References

1. Kumar G, Reddy KR, Foster C. Modeling elasto-visco-bio-plastic mechanical behavior of municipal solid waste in landfills. Acta Geotechnica. 2021;16(4):1061-81.
2. Jafari NH, Stark TD, Thalhamer T. Progression of elevated temperatures in municipal solid waste landfills. Journal of Geotechnical and Geoenvironmental Engineering. 2017;143(8):05017004.
3. Bouazza A, Nahlawi H, Aylward M. In situ temperature monitoring in an organic-waste landfill cell. Journal of Geotechnical and Geoenvironmental Engineering. 2011;137(12):1286-9.
4. Hoor A, Rowe RK, Pollard A, "A method for reducing the temperature of landfill liners in MSW landfills," in *Proceedings of the 1st Global Waste Management Symposium, Copper Mountain Conference Center, CO (CD-ROM)*, 2008.
5. Luettich SM, Yafrate N. Measuring Temperatures in an Elevated Temperature Landfill. Geo-Chicago 2016. 2016. p. 162-76.
6. Yesiller N, Hanson JL. Analysis of temperatures at a municipal solid waste landfill. 2003.
7. Yeşiller N, Hanson JL, Liu W-L. Heat generation in municipal solid waste landfills. Journal of Geotechnical and Geoenvironmental Engineering. 2005;131(11):1330-44.
8. Yoshida H, Rowe R, "Consideration of landfill liner temperature," in *Proceedings Sardinia*, 2003: Citeseer.
9. Zhou Y, Rowe RK. Modeling of clay liner desiccation. International Journal of Geomechanics. 2005;5(1):1-9.
10. Azad FM, El-Zein A, Rowe RK, Airey DW. Modelling of thermally induced desiccation of geosynthetic clay liners in double composite liner systems. Geotextiles and Geomembranes. 2012;34:28-38.
11. Southen J, Rowe R. Numerical modelling of thermally induced desiccation of geosynthetic clay liners observed in laboratory experiments. Geosynthetics International. 2011;18(5):289-303.
12. Southen J, Rowe RK. Modelling of thermally induced desiccation of geosynthetic clay liners. Geotextiles and Geomembranes. 2005;23(5):425-42.
13. Azad FM, Rowe RK, El-Zein A, Airey DW. Laboratory investigation of thermally induced desiccation of GCLs in double composite liner systems. Geotextiles and Geomembranes. 2011;29(6):534-43.
14. Hoor A, Rowe RK. Potential for desiccation of geosynthetic clay liners used in barrier systems. Journal of Geotechnical and Geoenvironmental Engineering. 2013;139(10):1648-64.
15. Southen JM, Rowe RK. Laboratory investigation of geosynthetic clay liner desiccation in a composite liner subjected to thermal gradients. Journal of Geotechnical and Geoenvironmental Engineering. 2005;131(7):925-35.
16. Abd El-Salam MM, Abu-Zuid GI. Impact of landfill leachate on the groundwater quality: A case study in Egypt. Journal of advanced research. 2015;6(4):579-86.
17. Yadav H, Kumar P, Singh V, "Hazards from the Municipal Solid Waste Dumpsites: A Review," in *International Conference on Sustainable Waste Management through Design*, 2018, pp. 336-42: Springer.
18. Sanchez M, Atique A, Kim S, Romero E, Zielinski M. Exploring desiccation cracks in soils using a 2D profile laser device. Acta Geotechnica. 2013;8(6):583-96.
19. El-Zein A, Airey D, Yu B, Esgandani GA, Proust G, Dias-da-Costa D, et al. Self-repair of cracks and defects in clay: a review of evidence, mechanisms, theories and nomenclature. Acta Geotechnica. 2021;16(12):3741-60.
20. Abeyrathne W, Priyankara N, Pushpakumara K, Ranaweera R, Alagiyawanna A. Suitability of expansive soil to use as clay liners in arid zone of Sri Lanka. 2012.
21. Met İ, Akgün H. Geotechnical evaluation of Ankara clay as a compacted clay liner. Environmental Earth Sciences. 2015;74(4):2991-3006.

22. Rushbrook P, Pugh M. Solid waste landfills in middle and lower-income countries: a technical guide to planning, design, and operation. The World Bank; 1999.
23. Widomski MK, Stępniewski W, Musz-Pomorska A. Clays of different plasticity as materials for landfill liners in rural systems of sustainable waste management. Sustainability. 2018;10(7):2489.
24. Shankar U, Muthukumar M, "Comprehensive review of geosynthetic clay liner and compacted clay liner," in *IOP conference series: materials science and engineering*, 2017, vol. 263, no. 3, p. 032026: IOP Publishing.
25. UNDESA, United Nations Department of Economic and Social Affairs. World Economic Situation and Prospects 2021. United Nations; 2021.
26. Holzlöhner U. Moisture Behaviour of Soil Liners and Subsoil beneath Landfills. Landfilling of Waste: Barriers. 2020:247-58.
27. Holzlöhner U, Schossig W, Wuttke W, Ziegler F. Long-term behaviour of earthen layers in landfill basal liners, moisture balance under thermal effects. Advanced landfill liner systems. Thomas Telford Publishing; 1997. p. 193-201.
28. Abdulrahman A. Hydraulic Performance of Compacted Clay Liners (CCLS) Under Simulated Landfill Conditions. Carleton University; 2014.
29. El-Zein A, Yu B, Ghavam-Nasiri A, "Insights into desiccation and self-healing of bentonite in geosynthetic clay liners under thermal loads," in *E3S Web of Conferences*, 2019, vol. 92, p. 03006: EDP Sciences.
30. Yu B, El-Zein A, Rowe RK, "Effect of bentonite mass per unit area on the desiccation of geosynthetic clay liners under high temperature and low overburden pressure," in *11th Intern Conf on Geosynth*, 2018.
31. Bouazza A, Ali MA, Rowe RK, Gates WP, El-Zein A. Heat mitigation in geosynthetic composite liners exposed to elevated temperatures. Geotextiles and Geomembranes. 2017;45(5):406-17.
32. Yu B, El-Zein A. Experimental investigation of the effect of airgaps in preventing desiccation of bentonite in geosynthetic clay liners exposed to high temperatures. Geotextiles and Geomembranes. 2019;47(2):142-53.
33. Yu B, El-Zein A, Rowe RK. Effect of added polymer on the desiccation and healing of a geosynthetic clay liner subject to thermal gradients. Geotextiles and Geomembranes. 2020;48(6):928-39.
34. Yu B, El-Zein A. Irrigated composite liner designs for fast hydration and prevention of thermal desiccation of geosynthetics clay liners. Geotextiles and Geomembranes. 2020;48(6):950-61.
35. Hoor A. Effects of temperature on the service-life of landfill liners and potential temperature control strategies. 2011.
36. Rowe RK, Hoor A, Pollard A. Numerical examination of a method for reducing the temperature of municipal solid waste landfill liners. Journal of Environmental Engineering. 2010;136(8):794-803.
37. Rowe RK, Pollard A, Chong A, Chisholm E, Toda R, Tomson C. Sustainable landfills–A technique for extracting heat to prolong service-life of geomembrane liners. Proceedings OttawaGeo. 2007:1310-4.
38. Hoor A, Rowe R. Application of thermal insulation in landfill liners. Geo-Frontiers 2011: Advances in Geotechnical Engineering. 2011. p. 1034-44.
39. Hoor A, Rowe RK. Application of tire chips to reduce the temperature of secondary geomembranes in municipal solid waste landfills. Waste management. 2012;32(5):901-11.
40. Rowe R, Hoor A. Predicted temperatures and service lives of secondary geomembrane landfill liners. Geosynthetics International. 2009;16(2):71-82.

907 41. Emmanuel E, Lau CC, Anggraini V, Pasbakhsh P. Stabilization of a soft marine clay using
908 halloysite nanotubes: A multi-scale approach. Applied Clay Science. 2019;173:65-78.
909 42. Anggraini V, Asadi A, Syamsir A, Huat BB. Three point bending flexural strength of
910 cement treated tropical marine soil reinforced by lime treated natural fiber. Measurement.
911 2017;111:158-66.
912 43. Anuar N, Chan C, "Reuse of dredged marine soils as landfill liner: effect of pH on
913 Escherichia coli growth," in *IOP Conference Series: Materials Science and Engineering*, 2017,
914 vol. 271, p. 012071.
915 44. Chalermyanont T, Arrykul S, Charoenthaisong N. Potential use of lateritic and marine clay
916 soils as landfill liners to retain heavy metals. Waste Management. 2009;29(1):117-27.
917 45. Emmanuel E, Anggraini V, Raghunandan ME, Asadi A. Utilization of marine clay as a
918 bottom liner material in engineered landfills. Journal of Environmental Chemical Engineering.
919 2020;8(4):104048.
920 46. Rahman Z, Yaacob W, Rahim S, Lihan T, Idris W, Mohd Sani W. Geotechnical
921 characterisation of marine clay as potential liner material. Sains Malaysiana. 2013;42(8):1081-
922 9.
923 47. Sandhya R, Shiva CV. Suitability of soft clay as clay liner based on clay-leachate
924 interaction studies. Journal of Mechanical and Civil Engineering. 2017;14(3):115-23.
925 48. Sobha C, Jose BT. Studies on the development and control of desiccation cracks in
926 compacted clay liner soils. Cochin University of Science & Technology; 2008.
927 49. Azme M, Murshed F, "Treatability of stabilize landfill leachate by using pressmud ash as
928 an adsorbent," in *IOP Conf Ser Earth Environ Sci*, 2018, vol. 140, pp. 12-41.
929 50. Chou L, Tun P. Conserving reefs beside a marine landfill in Singapore. Coral Reefs.
930 2007;26(3):719.
931 51. Kamon M, Zhang H, Katsumi T. Redox effects on heavy metal attenuation in landfill clay
932 liner. Soils and Foundations. 2002;42(3):115-26.
933 52. Sridharan A, Sivapullaiah PV. Mini compaction test apparatus for fine grained soils.
934 Geotechnical Testing Journal. 2005;28(3):240-6.
935 53. Ben Cheikh El Hocine H, Touafek K, Kerrour F. Theoretical and experimental studies of a
936 new configuration of photovoltaic–thermal collector. Journal of Solar Energy Engineering.
937 2017;139(2).
938 54. Mendrinos D, Katsantonis S, Karytsas C. Review of Alternative Pipe Materials for
939 Exploiting Shallow Geothermal Energy. Innovations in Corrosion and Materials Science
940 (Formerly Recent Patents on Corrosion Science). 2017;7(1):13-29.
941 55. Saber M. Bending Test and Simulation of Welded Galvanized Steel Pipes. Tehnički
942 vjesnik. 2021;28(2):509-14.
943 56. Touafek K, Kerrour F, Haloui H, Khelifa A. Model validation of an empirical photovoltaic
944 thermal (PV/T) collector. Energy Procedia. 2015;74:1090-9.
945 57. Touafek K, Khelifa A, Adouane M. Theoretical and experimental study of sheet and tubes
946 hybrid PVT collector. Energy Conversion and Management. 2014;80:71-7.
947 58. Coccia CJ, Gupta R, Morris J, McCartney JS. Municipal solid waste landfills as geothermal
948 heat sources. Renewable and sustainable energy reviews. 2013;19:463-74.
949 59. Faitli J, Erdelyi A, Kontra J, Magyar T, Varfalvi J, Muranyi A, "Pilot scale decomposition
950 heat extraction and utilization system built into the “Gyal Municipal Solid Waste Landfill”,"
951 in *Proceedings of 15th International Waste Management and Landfill Symposium, Cagliari,*
952 *Italy*, 2015.
953 60. Benson CH, Daniel DE, Boutwell GP. Field performance of compacted clay liners. Journal
954 of Geotechnical and Geoenvironmental Engineering. 1999;125(5):390-403.
955 61. Daniel DE, Benson CH. Water content-density criteria for compacted soil liners. Journal
956 of Geotechnical Engineering. 1990;116(12):1811-30.

957 62. Hirebelaguly Shivaprakash S, Sridharan A. Correlation of compaction characteristics of
958 standard and reduced Proctor tests. Proceedings of the Institution of Civil Engineers-
959 Geotechnical Engineering. 2021;174(2):170-80.
960 63. Huang Z, Wei B, Zhang L, Chen W, Peng Z. Surface crack development rules and shear
961 strength of compacted expansive soil due to dry–wet cycles. Geotechnical and Geological
962 Engineering. 2019;37(4):2647-57.
963 64. Rayhani MT, Sarabadani H. Factors affecting hydration of Geosynthetic Clay Liners in
964 landfill applications. 2013.
965 65. Southen JM, Rowe RK. Investigation of the behavior of geosynthetic clay liners subjected
966 to thermal gradients in basal liner applications. ASTM International; 2004.
967 66. Çengel Y, Ghajar A. Heat and mass transfer: Fundamentals and applications. Fifth edition
968 ed. McGraw-Hill Education; 2015.
969 67. Onnen MT. Thermal Numerical Analysis of Vertical Heat Extraction Systems in Landfills.
970 2014.
971 68. Dombaycı ÖA, Gölcü M, Pancar Y. Optimization of insulation thickness for external walls
972 using different energy-sources. Applied Energy. 2006;83(9):921-8.
973 69. Sisman N, Kahya E, Aras N, Aras H. Determination of optimum insulation thicknesses of
974 the external walls and roof (ceiling) for Turkey's different degree-day regions. Energy Policy.
975 2007;35(10):5151-5.
976 70. Yildiz A, Gurlek G, Erkek M, Ozbalta N. Economical and environmental analyses of
977 thermal insulation thickness in buildings. Journal of Thermal Science and Technology.
978 2008;28(2):25-34.
979 71. SRS1 Software LLC. SRS1 Cubic Spline for Excel 2.5.1.0 ed.
980 http://www.srs1software.com/SRS1CubicSplineForExcel.aspx: SRS1 Software, LLC; 2015.
981 72. Southen J, Rowe R, "Desiccation behaviour of composite landfill lining systems under
982 thermal gradients," in *Proc International Symposium on Clay Geosynthetic Barriers,*
983 *Nuremberg, AA Balkema*, 2002.
984 73. Mitchell JK, Soga K. Fundamentals of soil behavior. John Wiley & Sons New York; 2005.
985 74. Selker J, Or D. Heat Flow and Thermal Effects in Soils. Soil Hydrology and Biophysics.
986 2021.
987 75. Simpson JR. Soil Heat Flow. Physical Processes in Terrestrial and Aquatic Ecosystems,
988 Transport Processes. 1977.
989 76. Blanco-Canqui H. Biochar and soil physical properties. Soil Science Society of America
990 Journal. 2017;81(4):687-711.
991 77. Liu Z, Xu J, Li X, Wang J. Mechanisms of biochar effects on thermal properties of red soil
992 in south China. Geoderma. 2018;323:41-51.
993 78. Al-Homoud MS. Performance characteristics and practical applications of common
994 building thermal insulation materials. Building and environment. 2005;40(3):353-66.
995 79. Noorollahi Y, Saeidi R, Mohammadi M, Amiri A, Hosseinzadeh M. The effects of ground
996 heat exchanger parameters changes on geothermal heat pump performance–A review. Applied
997 Thermal Engineering. 2018;129:1645-58.

998